Sensitivity of Cerebellar Reaching Ataxia to Kinematic and Dynamic Demands

Kyunggeune Oh [a, b], Di Cao [c, d], Noah Cowan [c, d], and Amy Bastian [a, b]
a. Center for Movement studies, Kennedy Krieger Institute, Baltimore, Maryland
b. Department of Neuroscience, Johns Hopkins University, Baltimore, Maryland
c. Department of Mechanical Engineering, Johns Hopkins University, Baltimore, Maryland
d. Laboratory for Computational Sensing and Robotics, Johns Hopkins University, Baltimore, Maryland

Abstract

Individuals with cerebellar ataxia often face significant challenges in controlling reaching, especially when multi-joint movements are involved. This study investigated the effects of kinematic and dynamic demands on reaching movements by individuals with cerebellar ataxia and controls using a virtual reality task. Participants reached target locations designed to elicit a range of coordination strategies between shoulder and elbow joint movements. The hand paths of the cerebellar group exhibited greater initial reaching direction error, larger trajectory curvature, and more inter-subject variability compared to controls. Kinematic simulations indicated that early hand movement errors were sensitive to the required onset times and rates of joint movements and were most impaired when opposite direction joint movements were required (e.g., elbow extension with shoulder flexion). This highlights significant disruptions in multi-joint motion planning and/or feedforward control in the cerebellar group. Dynamic analysis showed that cerebellar participants' movements were more impaired in reaching directions where interaction torques would normally assist the desired elbow and shoulder movements, which required them to rely more on muscle torques to move. These reach directions were also those that required opposite direction joint movements. Overall, our data suggest that reaching deficits in cerebellar ataxia result from 1) the early-phase motion planning deficits that are exacerbated by stringent timing coordination requirements and 2) the inability to compensate for interaction torques, particularly when they assist the intended movement.

Introduction

A hallmark of cerebellar damage is movement incoordination (ataxia). For example, people with ataxia reach with hand paths that show abnormal curvature and oscillation as they home in on a target. Many studies have quantified kinematic abnormalities in an effort to understand the fundamental motor control deficits associated with reaching ataxia. Some studies have used reductionist methods by physically constraining movement to a single-joint (e.g., elbow) and shown kinematic abnormalities including some dysmetria (i.e. over- or undershooting), oscillation, and prolonged deceleration phases (Bhanpuri et al. 2014; Hallett and Massaquoi 1993; Zimmet et al. 2020). Several groups have reported that multi-jointed reaches are more

impaired than single-jointed reaches, due to abnormal coordination between joints (Bastian and Thach 1995; Goodkin et al. 1993; Thach et al. 1992). Consistent with this, it has been found that a single jointed elbow movement worsens when it is made without shoulder constraint, due to poor shoulder stabilization (Bastian et al. 2000). These findings suggest that coordination problems associated with cerebellar ataxia may stem from poor control of the more complicated kinematics and dynamics of multi-jointed movements.

One hypothesis is that ataxia may arise due to poor control of specific elements of movement dynamics. People with cerebellar ataxia have been reported to have difficulty predicting and accounting for "interaction torques", torques produced at a given joint (e.g. elbow) by motions of other linked joints (e.g. shoulder) (Bastian et al. 1996; Topka et al. 1998a; Topka et al. 1998b). Interaction torques scale with movement velocity and acceleration. They can induce large accelerations across joints, powerfully affecting reaching trajectories. Accordingly, when people with cerebellar ataxia make faster reaching movements, they show greater overshooting errors caused in part by poor compensation for interaction torques (Bastian et al. 1996; Topka et al. 1998a; Topka et al. 1998b). Interaction torques also exhibit nonlinear characteristics, depending on the number of joints involved, their initial configurations, and relative movement directions (Bastian et al. 2000; Gribble and Ostry 1999; Hollerbach and Flash 1982). Importantly, depending on the reaching direction, interaction torques can assist or resist desired joint motions (Galloway and Koshland 2002). Typical adults can predictively utilize or counteract interaction torques to make a well-coordinated reach (Maeda et al. 2017). It is not clear if people with cerebellar ataxia show different patterns of deficit depending on whether interaction torques assist or resist the desired joint motions in reaching.

Impaired dynamic control may explain why people with cerebellar damage show errors early in reaching that vary with movement direction (Germanotta et al. 2015; Gibo et al. 2013; Maschke et al. 2004; Zimmet et al. 2019). This has been observed in several studies that used a "center-out" reaching tasks in the horizontal plane, with equidistant targets from a central starting point, like a clock face. Using this task, people with ataxia can make early reaching errors rotated clockwise or counterclockwise relative to the desired target (e.g., Gibo et al. 2013). Each of the aforementioned studies noted that some reaching directions appeared "easier" than others—people with cerebellar damage could reach directly to some targets but showed large errors for other targets. It is difficult to find a systematic pattern across these studies because they used different initial starting positions, different numbers and positions of targets and involved different robots that altered the inertia of the arm.

Here we were interested in understanding if people with cerebellar ataxia show different sensitivities to the kinematic and dynamic demands of reaches made with different combinations of joint movements. We used virtual reality to display reaching targets that were classified according to the direction and combination of standard 20-degree shoulder and 20-degree elbow joint motions. Some combinations required tight control of the timing and rate of

shoulder and elbow kinematics for reaching, whereas others did not. In addition, some combinations involved interaction torques that assisted the desired joint motions for reaching, whereas others involved resistive interaction torques. Although interaction torques can be accentuated by fast movements, facilitating analysis (Bastian et al. 1996; Bastian et al. 2000; Becker et al. 1991; Haggard et al. 1994; Topka et al. 1998a; Topka et al. 1998b), natural arm reaching speeds can nevertheless elicit them (Bhanpuri et al. 2014; Hallett and Massaquoi 1993; Zimmet et al. 2020). Thus, we focus here on reaching movements that were at natural and comfortable speeds, as such movements may provide the most insight into everyday activities performed by individuals with cerebellar ataxia.

Materials and methods

Subjects

Seventeen control subjects and sixteen individuals with cerebellar ataxia were enrolled in this study. All participants were right-handed, and control subjects were matched to cerebellar ataxia subjects in terms of age and sex, as detailed in Table 1. The Scale for the Assessment and Rating of Ataxia (SARA) was employed to evaluate the severity of ataxia in all cerebellar patients. The assessments were conducted remotely via Zoom video calls (Zoom Video Communications, Inc., San Jose, CA, USA), using dual-camera angles: one from the laptop's built-in camera facing the subjects and another from a webcam positioned to their right side. Note that remote administration of the SARA has been shown to be valid and reliable (Reoli et al. 2024). Subjects with severe ataxia were accompanied by a caregiver during the assessment. Informed consent was secured from all participants in this study. A summary of the cerebellar subjects' information can be found in Table 2.

Table 1. Subject information

Group	Controls	Ataxia
Headcount	17	16
Age	61.6 (±6.9)	60.0 (±11.9)
M/F	7/10	5/11
Body Weight (lbs)	164 (±26)	157 (±29)
UA segment length (cm)	31.7 (±2.6)	31.6 (±1.9)
LA segment length (cm)	39.8 (±2.8)	39.5 (±2.0)

Table 2. Characteristics of patients with cerebellar damage

Subject	Age	Sex	Diagnosis	Total SARA (/40)	Arm-related SARA (/12)
01	69	M	SCA-27B ADCA3	3.5	1
02	69	F	SCA6	26	7
03	68	M	SCA6	26	7
04	50	F	SCA2	19	6.5
05	61	F	SCA6	29	7
06	68	F	EA2	13	4
07	42	F	SCA3	19	1.5
08	57	M	Sporadic, episodic	16.5	3
09	72	M	SCA5	24	7
10	50	F	SCA8	13	3.5
11	42	F	SCA3	24	8
12	54	F	Unknown etiology	13.5	2.5
13	80	F	SCA6	17	5
14	61	F	SCA5	30	8
15	73	F	SCA6	15.5	5
16	44	M	SCA8	14	4

Apparatus

We designed a remote data collection system that was delivered to each participant's home, during the COVID-19 pandemic. This allowed us to study people with cerebellar ataxia who lived far away from the lab—our subjects were located in Maryland, Virginia, Vermont, North Carolina Tennessee, Florida, Illinois, Missouri and California. The data collection equipment package included an Oculus Rift S virtual reality (VR) device (Meta Reality Labs, WA, USA) for hand movement measurement, a Logitech C922 webcam for monitoring subjects' sagittal view, and a gaming laptop that was used to control the VR system, perform data collection, and to conduct the video call. The data collection rate for the webcam and VR device was 30Hz. Participants received a detailed set of instructions on how to connect all equipment with color coded cables and photographs. After the computer was connected to the internet, the remaining equipment set up was guided by investigators through a video call and remote

control of the laptop using TeamViewer (Google LLC, CA, USA). During testing, subjects sat in a stable chair with their feet on the floor wearing the Oculus Rift. The laptop sat on a stable surface in front of them and the webcam was positioned to capture a view of their right side in the sagittal plane. The hand movement was recorded by the Rift S VR, with 30Hz sampling rate. The joint motions of the shoulder and elbow were also monitored and recorded by the webcam at 30Hz frame rate. All ataxic participants were tested off site. Control participants were tested either off- or on-site. If on-site, the subjects were not involved in setting up the devices. Otherwise, all testing procedures were identical.

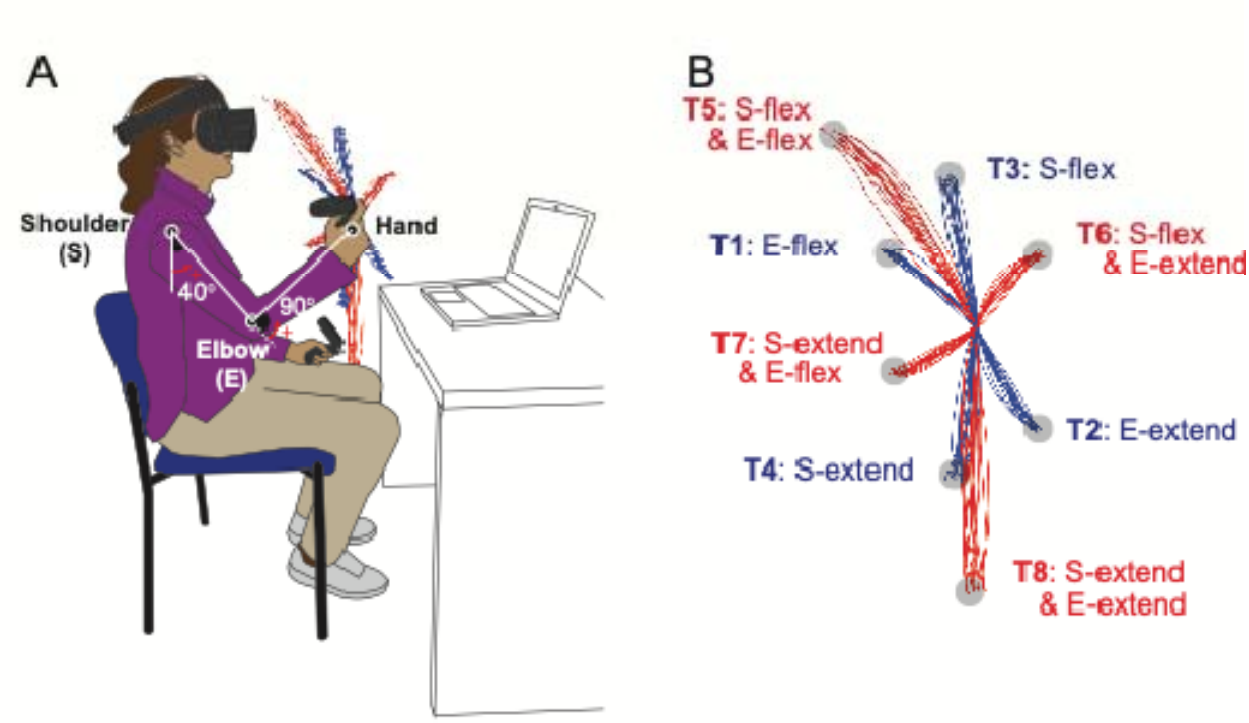

Figure 1. Task Diagram. A. Initial Position: The shoulder joint is angled at 40 degrees from the ground direction, and the elbow joint is at 90 degrees, positioning the hand at the height of the right shoulder. The positive direction for the joint angles is counterclockwise when viewed from the right. B. Target Locations: The starting point and all targets are located on a sagittal plane that aligns with the right shoulder. Hand paths leading to four single-joint targets are illustrated in red, while those leading to four double-joint targets are indicated in blue.

Subject calibration

Before beginning the reaching study, each subject was asked to have another person measure lengths of their arm segments, including the upper arm segment (from the acromion to radiale) and the lower arm and hand segment (from radiale to proximal interphalangeal joint of the index finger). This was done while we were online with the subject, providing verbal instructions and video check. The subject was then instructed to sit on a chair and maintain a fixed trunk and head position during the task either by leaning on the back of the chair or sitting upright.

In the initial stage of the VR task, all subjects underwent a calibration process. They put on the VR headset and held a VR controller in each hand. Participants were told that the (virtual) green arrows marked on the floor pointed in the direction that they should be facing; after verifying that they were facing the correct direction, they were asked to raise both hands (which were holding the VR controllers) to the height of their shoulder and extend them forward shoulder-width apart. The position of the right shoulder in 3D space was estimated by recording the positions of the controllers and utilizing the measured lengths of the arm segments.

Paradigm

Participants performed goal-directed arm reaching movements in the sagittal plane in front of their right shoulders. The starting position of the arm reach was defined with the elbow joint angle at 90 degrees and the shoulder joint angle at 40 degrees relative to the ground, as shown in Figure 1. Reaches were performed to eight targets that were displayed one at a time during the task. Targets were located in the vertical plane, with four of them being single-joint targets that could be reached with 20 degrees of excursion in either flexion or extension of the shoulder or elbow joint.

The remaining four targets were two-joint targets, requiring 20 degrees of joint excursions in both the shoulder and elbow joints, flexion or extension. Note that we use the term "opponent joint movements" for two-joint reaches where shoulder and elbow joints moved in opposite directions (e.g. shoulder flexion with elbow extension and vice versa) and "same-direction joint movements" when both joints were flexing or extending. A trial was defined as a single reaching movement from the starting position to one of the targets. Before data collection, the subjects performed practice trials until they became accustomed to the reaching task. For data collection, participants reached nine times to each of the 8 targets resulting in 72 total trials arranged in a pseudo-random manner.

Each trial began by displaying the starting point, a red sphere with 2 cm radius, with a gray wire frame surrounding it. The subject's hand (the right VR controller) position was displayed as a white sphere with a 1.5 cm radius. When the subject's hand remained inside the red sphere for two seconds, the wire frame surrounding the start point changed from gray to green, a target then appeared in the sagittal plane, and the starting point disappeared. At this point, participants were instructed to reach the target with their natural arm reaching speed, using a straight hand path. All targets were 2-cm radius spheres of different colors (other than red) and were surrounded by a wire frame that changed its color from gray to green if the hand was in the target. After two seconds, the target disappeared, and the starting point was displayed. The task was repeated in this way for a total of 72 targets. There was no time limit for each reach. The subject took breaks anytime between trials for as long as they wanted. The total task took

about ~20-30 mins, and most of subjects took ~1-2 breaks that were typically over within 5 minutes.

Data analysis

Hand paths

Hand position and velocity were lowpass filtered with a 10Hz cut-off frequency using the 'lowpass' function of Matlab. A Hampel filter was also applied to the data using 'hampel' function of Matlab with a window size 5 to remove and interpolate the occasional outlier data point within a trial. The onset and offset timings of each trial were defined with 10% of the peak hand velocity.

We calculated kinematic parameters within the sagittal plane that reflected different aspects of the reaching movement. The initial direction of the hand was quantified as the angle formed between a straight line from start to target and hand to target at 67 milliseconds (equivalent to 2 data frames) after the onset of the reaching movement. The initial hand direction is a critical measure as it reflects the subject's motion planning and the efficiency of their feedforward control during the early phase of the reaching movement (Alhussein and Smith 2021; Haith et al. 2015). The maximum deviation ratio was used to represent curvature of the hand path. It was calculated as the perpendicular distance from a line connecting the start and end target to the farthest deviation of the hand path. This value was normalized to the distance from start to end target. A path length ratio was used to evaluate the kinematic efficiency of the hand movement. It was calculated by dividing the actual distance traveled by the hand by the straight-line distance between the start and the end target. Efficient kinematics (lower path ratio) refers to movements that go straight to the target, and inefficient kinematics (higher path ratio) follow a more circuitous (e.g., oscillatory) path to the target. Lastly, peak hand path velocities, as well as acceleration and deceleration times, were calculated.

Joint angles

Joint angles were calculated using inverse kinematics assuming purely sagittal plane motion (note that the average maximum out of plane motion was small, 0.78 cm for control group and 1.94 cm for cerebellar ataxia group). The participants' right shoulder was set as the origin of the coordinate system, with the anterior (+) – posterior (-) direction as the x-axis and the upward (+) – downward (-) direction as the y-axis. The hand position was denoted (X,Y). Using the given arm segment lengths L1 (upper arm) and L2 (lower arm and hand), the shoulder (θ_{SH}) and elbow (θ_{EL}) joint angles were calculated as follows:

$$\Theta_{EL} = \mathrm{acos}\left(\frac{X^2+Y^2-L1^2-L2^2}{2*L1*L2}\right) \quad (1)$$

$$\Theta_{SH} = \text{atan}\left(\frac{Y}{X}\right) - \text{atan}\left(\frac{L2*\sin\Theta_{EL}}{L1+L2*\cos\Theta_{EL}}\right) \quad (2)$$

The elbow and shoulder angles are depicted in Figure 1A.

Kinematic simulation

A kinematic simulation was conducted to examine the impact of coordination between the shoulder and elbow joints on hand movement during two-joint reaching movements (Figure 6). First, the elbow and shoulder trajectories are time-normalized for a given target and averaged on a subject-by-subject basis. We then averaged across control subjects to create mean shoulder and elbow joint motions. These were fit to a sigmoidal curve to calculate the amplitude (a), rate (r), and center point (c).

$$y = \frac{a}{1+e^{\left(-(t-c)*\frac{4r}{|a|}\right)}} \quad (3)$$

From this, we were able to systematically shift joint onset times and the relative rates of elbow and shoulder joint movements to determine effects on hand movement deviation. Note that the hand deviation angle was calculated at the 25% point of the target distance because it provided a good estimate of the rate of shoulder and elbow motions in-flight. This was done for all combinations of simulated two-joint motions as is depicted in the heatmaps shown in Figure 6. Finally, the relative onset time difference and relative rate ratio from individual control and cerebellar subject joint motions were plotted directly on the heatmap.

Joint torque

Joint torques were calculated using inverse dynamics equations (Bastian et al. 1996), and the calculations were based on estimations of mass and moment of inertia for each segment, (1) upper arm and (2) forearm and hand (Winter 1990). However, as wrist movement was restricted with a brace in this study, wrist angle, angular velocity, and angular acceleration were all assumed to be zero. Alternative text: We assumed wrist angle, angular velocity, and angular acceleration were all zero. The inverse dynamics calculations produced net torque (NET), gravity torque (GRAV), muscle torque (MUS), and interaction torque (INT). The basic torque equation used is NET = MUS – INT – GRAV. However, to capture the dynamic variations in the muscle torque components, we calculated the dynamic muscle torque (DMUS = MUS – GRAV), which represents the residual torque after subtracting the gravitational component (Yamasaki et al. 2008). To evaluate the relationship between dynamic muscle torque and interaction torque, we computed the zero-lag cross-correlation between DMUS and INT.

To assess the relative contributions of DMUS and INT to NET, we calculated the contribution index of DMUS and INT impulses to NET (Sainburg and Kalakanis 2000; Vu et al. 2016; Yamasaki et al. 2008). Note that torque impulse represents the integral of torque over a given time

interval. Time intervals during which INT took the same sign as NET were considered to contribute a positive interaction torque impulse, whereas intervals where INT opposed the NET were classified as contributing to a negative interaction torque impulse. The total interaction torque impulse, obtained by summing both positive and negative impulses over the movement duration, was divided by the absolute net impulse to calculate the contribution index of INT to NET. The DMUS impulse contribution to NET was computed similarly.

$$INT\ index = \frac{\int_{t_0}^{t_f} INT(t) \cdot sign(NET(t))dt}{\int_{t_0}^{t_f} abs(NET(t))dt} \tag{4}$$

$$DMUS\ index = \frac{\int_{t_0}^{t_f} DMUS(t) \cdot sign(NET(t))dt}{\int_{t_0}^{t_f} abs(NET(t))dt} \tag{5}$$

Noting that INT=NET-DMUS, the sum of the INT and DMUS indexes is always 1 as shown:

$$SUM = \frac{\int_{t_0}^{t_f} DMUS(t) \cdot sign(NET(t))dt + \int_{t_0}^{t_f} (NET(t) - DMUS(t)) \cdot sign(NET(t))dt}{\int_{t_0}^{t_f} abs(NET(t))dt}$$
$$= \frac{\int_{t_0}^{t_f} NET(t) \cdot sign(NET(t))dt}{\int_{t_0}^{t_f} abs(NET(t))dt} = \frac{\int_{t_0}^{t_f} abs(NET(t))dt}{\int_{t_0}^{t_f} abs(NET(t))dt} = 1 \tag{6}$$

Statistical analysis

A two-way ANOVA was conducted to examine the effects of the between-subjects factor (group: controls and cerebellar patients) and the within-subjects factor (target). For post hoc comparisons, a Bonferroni correction was applied. When we examine the correlations between variables, Pearson's correlation coefficient was employed. To ensure the robustness of this approach, we checked for homogeneity of variances between the variables using Levene's test.

Results

Hand kinematic analysis

Figure 2 shows hand paths of the control group and the cerebellar group. A thin line traces the average hand path curve for each subject, with blue indicating paths to targets reachable via one joint movement, and red indicating those to targets requiring two joint movements. The group average curves are depicted by bold black lines. Since all subjects had target locations adjusted for their arm segment lengths, the hand paths shown in this figure are scaled using the average target positions of each group, with the starting point positioned at the origin.

The cerebellar ataxia group exhibited higher inter-subject variation in hand path trajectories. In Figure 2, it is clear that the hand paths of the cerebellar group exhibited a greater degree of

subject-to-subject variation compared to the control group. This aligns with findings from previous research (Day et al. 1998; Therrien et al. 2021). The subject-to-subject variation of the hand paths was quantified using the standard deviation of maximum deviation (Table 3). Additionally, hand paths viewed from the front showed greater variation in the cerebellar group, yet overall, the hand paths of both groups generally remained near the target plane, as evidenced by Figure 2 (maximum out of plane deviation was < 2 cm, see methods).

The cerebellar group showed greater hand path curvature compared to controls, and this difference was largest during opponent joint movements (T6 and T7).

Recall that the targets were set based on joint motions—we studied different combinations of 20-degree elbow and/or shoulder joint movements. Two of these target movements, T6 and T7, required that participants simultaneously perform flexion in one joint and extension in the other. We refer to these as *opponent joint movements* for simplicity.

Figure 2 shows that the control group's hand paths were relatively straight for all targets, while the cerebellar group's paths were curved, a phenomenon consistent with similar observations reported in previous studies (Gibo et al. 2013; Zimmet et al. 2019). For both groups, the curvature was lowest in single joint movements and was greatest in two-joint movements where one joint flexed while the other extended (and vice versa, targets T6 and T7). The cerebellar group showed significantly higher maximum deviation ratio values compared to the control group ($F([1,248] = 113.47$, $p < 0.001$), with the difference most pronounced for targets T6 and T7 ($F([1,248] = 68.836$, Bonferroni post hoc test, $p < 0.001$; $F([1,248] = 91.527$, Bonferroni post hoc test, $p < 0.001$).

The second index utilized was the hand path ratio, which represents the relative increase in the actual path distance travelled by the hand compared to the direct distance from the starting point to the target. A perfect straight path would have a hand path ratio of 1; any deviation results in a ratio greater than 1. This metric serves as an indicator of the hand path curvature and is also interpretable as a measure of the efficiency of the reaching movement. The results, depicted in Figure 3B, demonstrate that for most targets, cerebellar patients' hand paths were longer than for control subjects ($F[1, 248]=97.754$, $p < 0.001$), with the most substantial differences again observed at targets T6 and T7 ($F([1,248] = 45.091$, Bonferroni post hoc test, $p < 0.001$; $F([1,248] = 48.363$, Bonferroni post hoc test, $p < 0.001$).

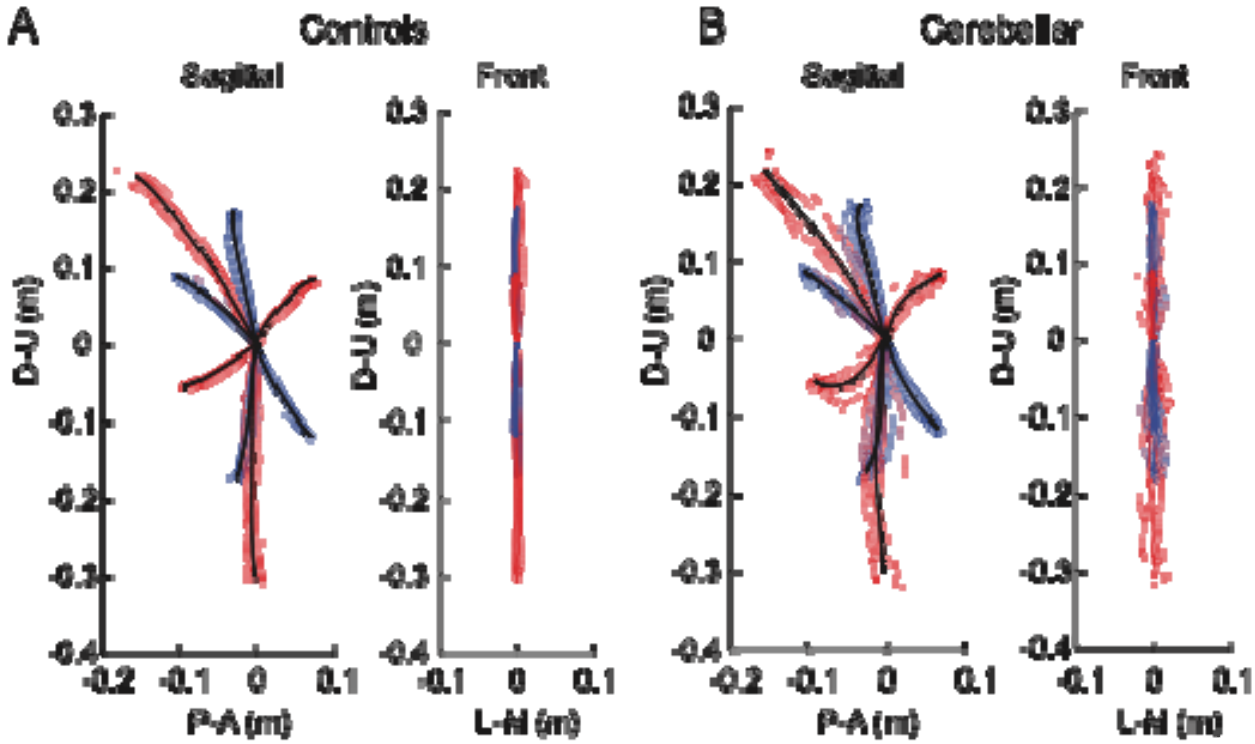

Figure 2. Hand paths. A. Mean hand path trajectories of all control subjects (left: sagittal view from the right; right: front view). B. Mean hand path trajectories of all cerebellar ataxia subjects (left: sagittal view from the right; right: front view). Individual lines represent the mean curves of each subject, and the thick black lines denote the mean trajectories of each subject group. The blue and red lines correspond to hand paths to single-joint and two-joint targets respectively. The hand trajectories of the different subjects were scaled to the average target distances of all subjects. Axes display directions: The Y-axis (up-down) and X-axis (anterior-posterior for sagittal view, medial-lateral for front view). Units are in meters.

The initial hand movement misdirection was largest for opponent joint movements (T6 and T7).

A significant difference in initial hand movement direction was observed between groups, but only for targets that required coordination of opponent joint movements (T6 and T7), as shown in Figure 3C ($F([1,248] = 11.263$, Bonferroni post hoc test, $p < 0.001$; $F([1,248] = 41.264$, Bonferroni post hoc test, $p < 0.001$). Note that positive values are clockwise rotations, and negative values are counterclockwise rotations from a line connecting the start to target positions. Representative hand paths from subjects in each group are illustrated in Figure 3D.

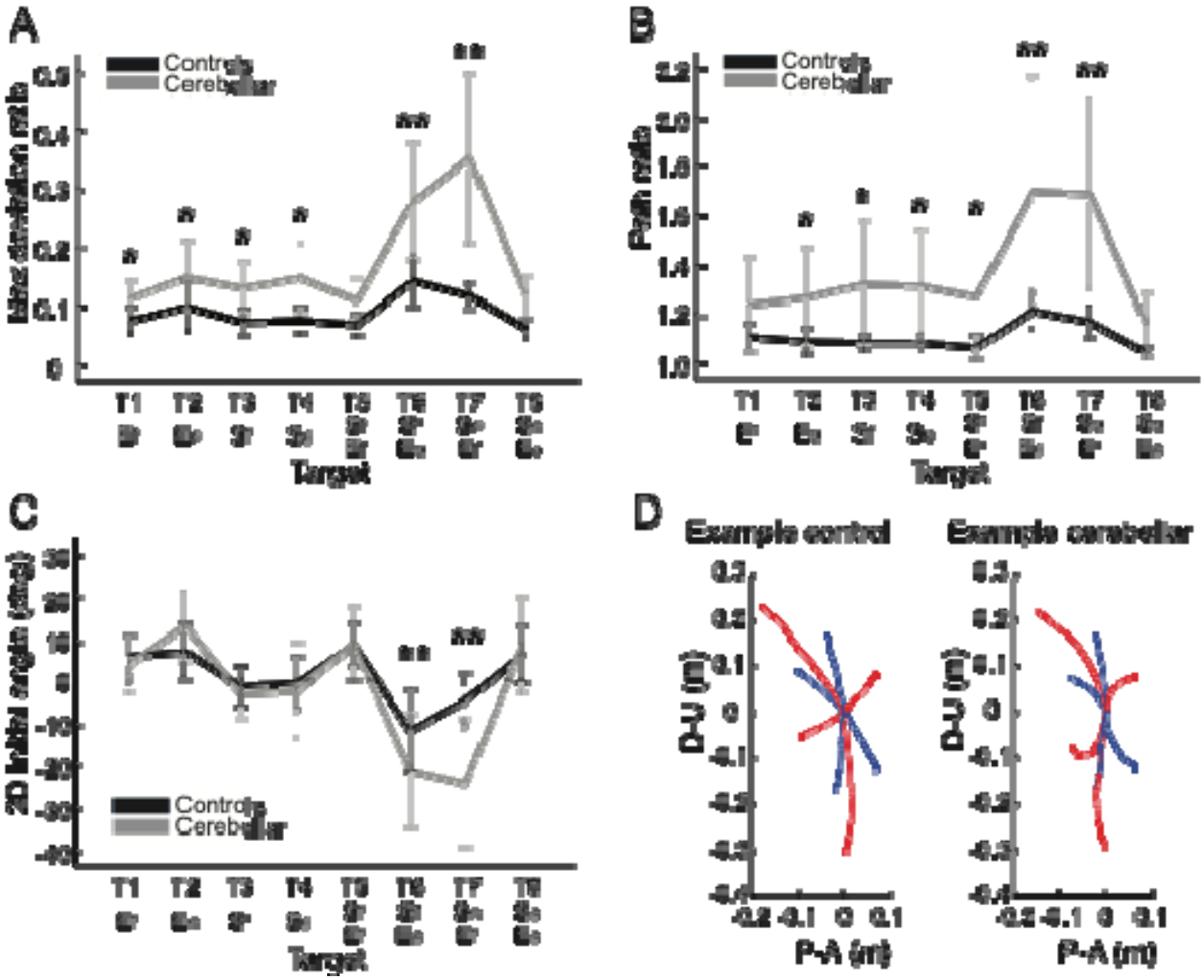

*Figure 3. Kinematic measures of hand path. A. Mean maximum deviation ratio. B. Mean path ratio. C. Mean 2D initial angle. The sign of hand movement and initial direction was defined as relative to the target direction connecting the start point and the target, with counterclockwise considered positive when viewed from the right side of the participants. *: p < 0.05, **: p < 0.001. D. Mean hand path trajectories of representative control and cerebellar ataxia subjects. The Y-axis represents upward (positive) and downward (negative) directions, and X-axis represents anterior (positive) and posterior (negative) directions, measured in meters. Blue and red lines represent hand trajectories to single-joint and two-joint targets, respectively.*

Table 3. Inter-subject variations of the hand paths: Standard deviations of maximum deviation ratio

	Target							
Group	1	2	3	4	5	6	7	8
Control	0.0237	0.0423	0.0224	0.0228	0.0191	0.0437	0.0223	0.0174
Cerebellar	0.0296	0.0638	0.0453	0.0612	0.0373	0.0991	0.1444	0.0362

People with cerebellar ataxia took longer to reach, with similar acceleration times but prolonged deceleration times. Total reach time, indicated by the entire height of the bar graph in Figure 4A, is defined as the duration from the onset to the offset of hand movement. The

cerebellar group's total reaching time was substantially longer compared to the control group ($F[1, 248]=88.176$, $p < 0.001$), mainly due to a longer deceleration time. While the acceleration time—defined as the duration from hand movement onset to peak hand velocity—was not significantly longer for the cerebellar group ($F[7, 248]=1.717$, $p=0.105$), the deceleration time—defined as the period from peak hand velocity to movement offset—exhibited a significant difference of 525 milliseconds ($F[7, 248]=5.341$, $p < 0.001$).

Peak hand velocities were similar between groups. As indicated in Figure 4B, the peak hand velocity between the two groups was found to be generally similar ($F[1, 248]=2.955$, $p=0.087$). In both groups, peak velocity increased proportionally to target distance, consistent with findings from previous goal-directed arm reaching studies (Gordon et al. 1994).

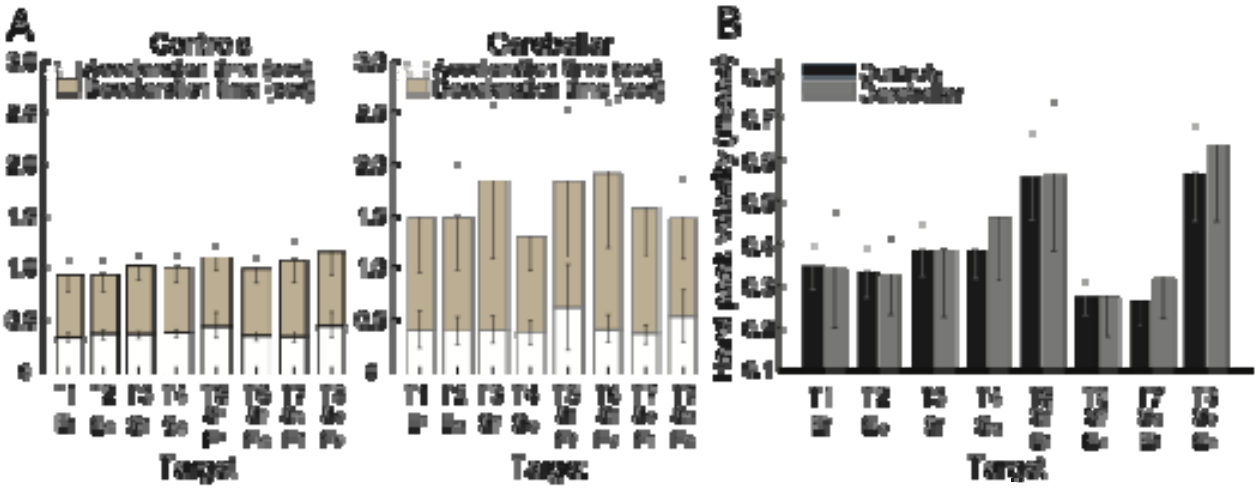

Figure 4. A. Acceleration, deceleration, and total reaching times (sec) for control and cerebellar ataxia groups. B. Peak hand velocity (m/sec) of controls and cerebellar groups for each target.

Arm joint kinematics analysis

Joint angle trajectories showed greater inter-subject variation in the cerebellar ataxia group, and this variation was more pronounced in the elbow. Figure 5A displays the time-normalized joint angle trajectories for all subjects. Time normalization was calculated by setting the arm reaching movement onset as 0% and the offset as 100%. Across the board, the trajectories exhibited a consistent joint excursion of approximately 20 degrees for each joint. However, in terms of trajectory variation, the cerebellar group demonstrated a higher level of variation compared to the control group. When comparing joints, both groups exhibited greater joint angle trajectory variation at the elbow than at the shoulder. The variation in joint angle trajectory was quantified using the standard deviation of the joint angle at the 50% mark on the normalized time axis, with the results depicted in Figure 5B.

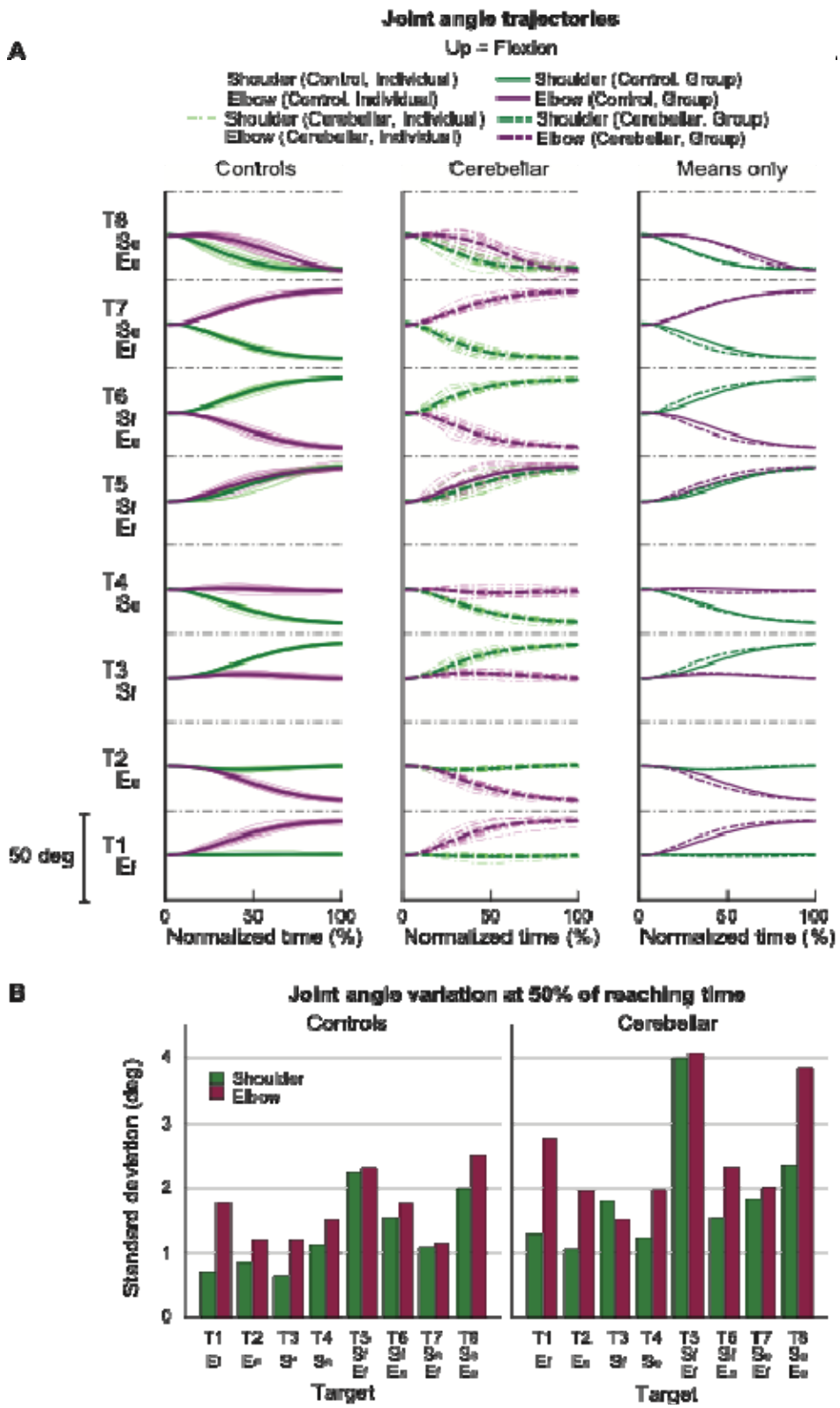

Figure 5. Joint angle trajectories and inter-subject variations. A. Joint angle trajectories for eight target locations, presented in the normalized time. The first and second columns display the individual mean and group mean trajectories for the control and cerebellar groups, respectively. Third column shows only group mean trajectories for both groups. B. Joint angle variation (in degree) measured by standard deviation of individual joint angles at 50% of reaching time.

Kinematic simulations of hand deviation for two-joint targets

Kinematic simulations reveal the sensitivity of hand path deviations to different patterns of shoulder and elbow coordination. Figure 6A-C illustrates how we altered the onset times or rates of shoulder movements relative to a standard elbow movement (examples taken from T6 which required shoulder flexion and elbow extension). The joint trajectories used in this simulation were from a logistic fit to the average joint motions of the control group (see Methods). We manipulated shoulder movement to have an earlier or later onset time relative to the elbow (Figure 6B), and a faster or slower rate of movement relative to that of the elbow (Figure 6C). Figures 6D and E show example hand paths resulting from different onset times or relative rates of joint motions for all four two-joint targets (T5-T8).

Figure 7 displays the complete colormaps of the kinematic simulations. The colors in the matrix represent the degree of hand deviation from the target direction, measured in degrees, at 25% of the reaching distance. These deviations are based on variations in relative joint onset times and rate changes (slopes) between the shoulder and elbow joints in control subjects. The X-axis shows the onset time difference between the shoulder and elbow joints, and a gray vertical line marks the average onset time difference of control subjects. The Y-axis displays the ratio of joint change rates between the shoulder and elbow joints, with the gray horizontal line representing the average rate ratio for the control group. Movements to Targets T5 and T8, show less sensitivity to relative onset times and rate ratios between joints, as indicated by the gradual shift in color across the maps. In contrast targets T6 and T7 are highly sensitive, as indicated by the abrupt changes in color across the maps.

We then individually marked each subject's joint onset time and joint change rate on the colormap, to compare the hand deviation predicted by the simulation with the hand deviation measured in the experiment. As shown in Table 4, the average difference between the two was 1.69 to 11.56 degrees for the control group and up to 2.62 to 15.79 degrees for the cerebellar ataxia group depending on the target locations, which can be visually confirmed by the color match between the individual data points and the colormap.

Controls tended to show tight control of the joints' onset times and rate ratios for targets T6 and T7, and looser control for targets T5 and T8. Thus, they appeared to take advantage of reduced precision requirements in joint control when they could, akin to the minimum intervention principle (Cashaback et al. 2015; Cusumano and Dingwell 2013). The degree of dispersion between individual subjects' data was represented by an 80% confidence interval error ellipse. Accordingly, for all four two-joint targets, it was observed that the cerebellar ataxia group's experimental data exhibited generally greater variation in both onset time differences and joint rate ratio differences compared to the control data. For target T6, the cerebellar group showed a tendency for earlier shoulder onset times, while for target T7, there was a tendency for a faster relative joint angle change rate in the shoulder.

Table 4. Simulated vs experimentally measured hand deviation angles (deg ± standard deviation)

Group	Target			
	5	6	7	8
Heathy	-4.28 ± 4.46	11.56 ± 12.40	1.69 ± 7.55	10.49 ± 8.38
Cerebellar	-2.62 ± 12.10	8.94 ± 18.32	5.45 ± 18.56	15.79 ± 13.68

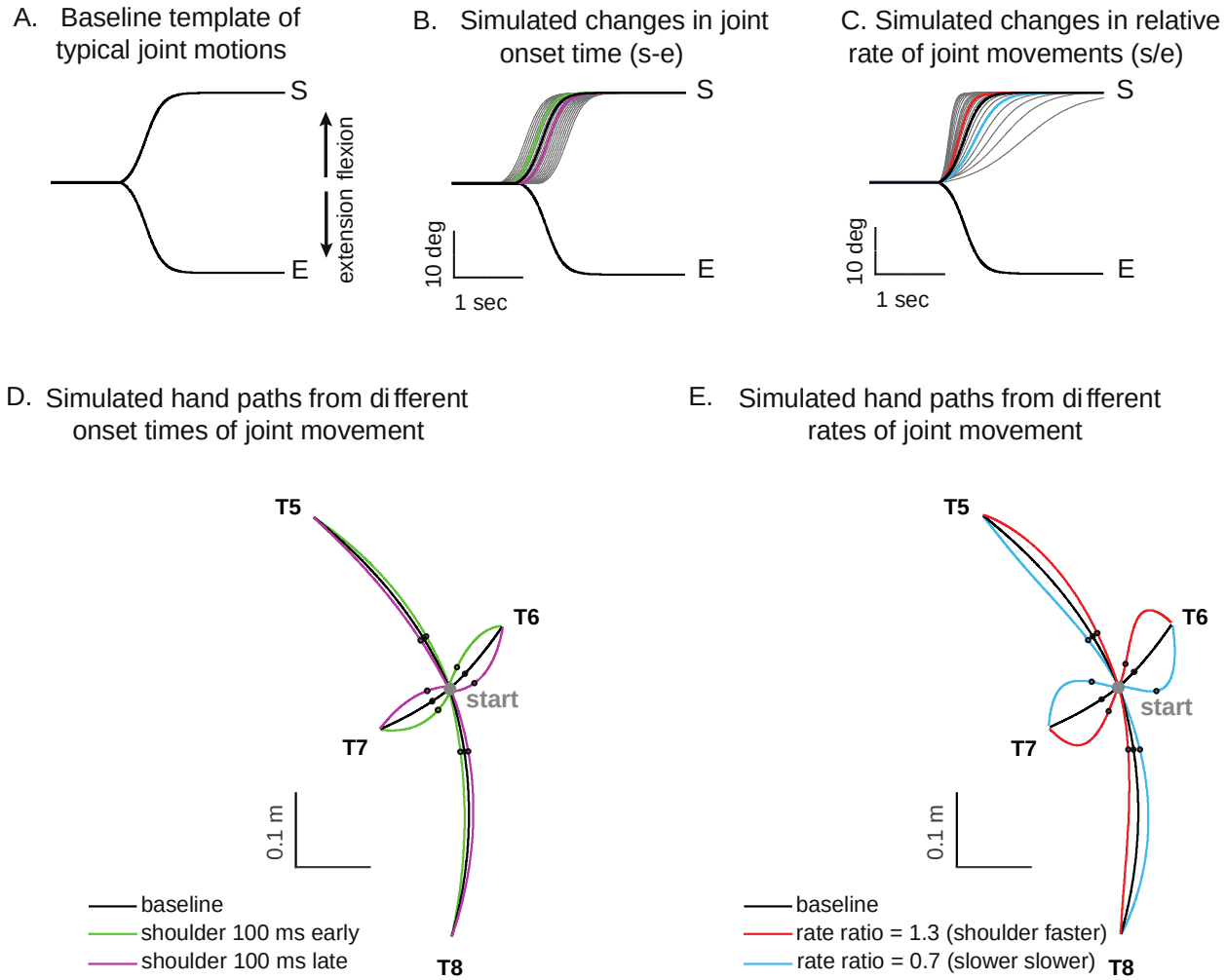

Figure 6. Simulated hand paths resulting from variations in shoulder and elbow joint movements. (A) Baseline template of typical joint motions (average joint motion of the control group). (B) Simulated changes in shoulder joint onset times. Shoulder joint angle trajectories with onset times 100 msec earlier or later than those of the elbow joint are shown in green and purple, respectively. (C) Simulated changes in the shoulder joint angle rates. The red and blue shoulder angle trajectories represent cases where the relative rate ratio between the shoulder and elbow are 1.3 and 0.7, respectively. (D, E) Joint angle trajectories over time for each condition. The black dots indicate the points where the hand reaches 25% of the distance from the starting position in the direction of the target. At these points, the hand's deviation angle from the target line was calculated.

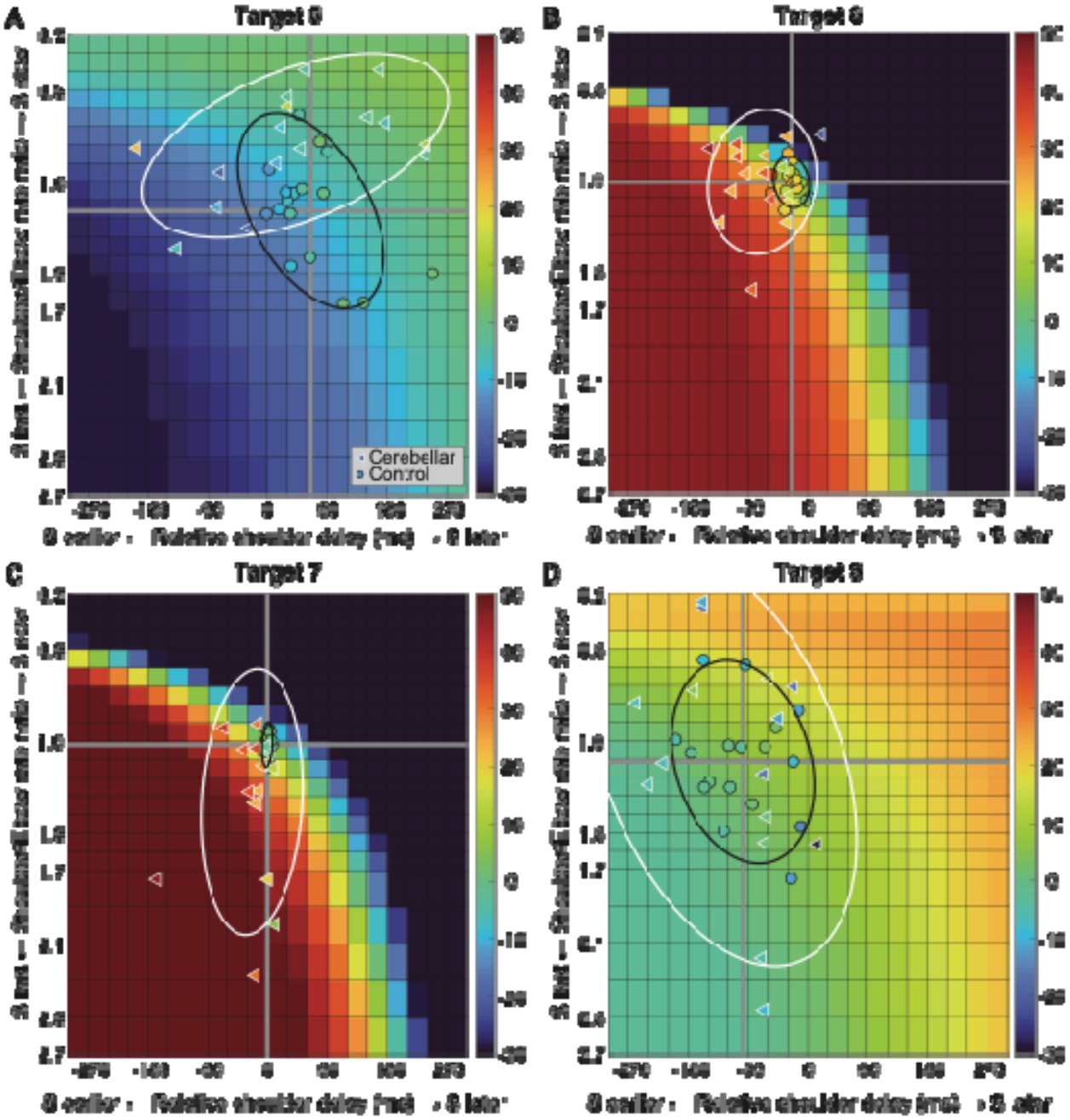

Figure 7. Kinematic simulations of the hand deviation from the target directions for two-joint targets: target T5 (A), T6 (B), T7 (C), and T8 (D). The simulated hand deviation from the target direction at 25% of the reaching distance is shown in degrees on colormaps and is based on variations in relative joint onset times and rate changes (slopes) between the shoulder and elbow joints in control subjects. The X-axis shows the onset time difference between the shoulder and elbow joints, where a gray vertical line represents the average onset time difference in controls. The Y-axis indicates the ratio of joint change rates between the shoulder and elbow joints, with a gray horizontal line representing the average rate ratio for the control group. Each subject's joint onset time and joint change rate are marked individually, enabling a comparison between the predicted hand deviation from the simulation and the measured hand deviation from the experiment.

Dynamic analysis

The torque patterns vary across two-jointed targets. Figure 8 presents the torque data for four two-joint targets, and illustrates the dynamic interplay between net, interaction, and dynamic muscle torques. As shown in the figure, the arm-reaching movements performed in this study were self-paced, leading to relatively smaller interaction torque compared to net torque and dynamic muscle torque. Additionally, across all four two-joint target movements, net torque and muscle torque exhibited similar patterns and magnitudes, indicating that muscle torque primarily contributed to overall movement. However, at the distal joint, the elbow, interaction torque was often comparable in magnitude to the other torques, especially when contrasted with the shoulder. While there were no significant differences in the overall pattern between the two groups, the cerebellar ataxia group demonstrated greater inter-subject variation and less smooth torque curves

The relationship between the torques varied depending on location of the target. Differences between control and cerebellar groups were less apparent. For targets T6 and T7 in particular—where the shoulder and elbow joints moved in opposite directions—interaction torque in both joints appeared to positively correlate with the other torques. This would imply that for these two targets, interaction torque acted in a manner that assisted the overall movement represented by net torque and the movement effort shown by muscle torque; this is examined in detail below.

Significant group differences were observed in the cross-correlation between interaction torque and dynamic muscle torques during opponent joint movements (T6 and T7). To quantitatively represent the relationship between the torques, we calculated the zero-lag cross-correlation between the dynamic muscle torque and the interaction torque to examine the simultaneous relationship between the torques. As shown in Figure 9, The cross-correlation values varied depending on the target location and joint movement combination. For the shoulder joint, a positive correlation between interaction torque and dynamic muscle torque was observed for targets T6 and T7, which required opponent joint movements, suggesting that the interaction torque aided shoulder movement. In contrast, at targets T5 and T8, the interaction torque appeared to hinder shoulder movement. These findings are consistent with the torque patterns shown in Figure 8. For the elbow joint, the interaction torque generally acted in a way that hindered elbow movement. However, in the control group's movement toward target T6, the relationship between the two showed a positive correlation, which was notably different from the cerebellar group.

The differences between the groups were most apparent at targets T6 and T7, where the shoulder joint showed a positive cross-correlation between interaction torque and dynamic muscle torque. At these two targets, the control group exhibited significantly higher cross-correlation values between shoulder interaction torque and dynamic muscle torque compared to the cerebellar group (T6: $F([1,248] = 21.986, p < 0.001$; T7: : $F([1,248] = 11.466, p < 0.001$).

This indicates that the control group was able to more effectively utilize interaction torques to assist joint movement, particularly at targets requiring complex, opposite movements between the elbow and shoulder. A difference between the groups was also observed at the elbow joint for target T7 ($F([1,248] = 67.346, p < 0.001$), but this was not the case for target T6.

There was a significant reduction in interaction torque contributions during opponent joint movements made by cerebellar patients (T6 and T7). Figure 10 illustrates the contribution index, which represents the relative contribution of interaction torque and dynamic muscle torque to net torque. Figure 8 shows that the interaction torque tended to assist the net torque for both shoulder and elbow joints, during arm reaching toward targets T6 and T7. This is indicated by positive contribution index values. In contrast, for targets T5 and T8, the contribution index of the interaction torque was close to zero or relatively low, indicating a minimal influence of the interaction torque on the net torque. In the case of dynamic muscle torque, both joints showed relatively high positive contribution index values, demonstrating a significant contribution to the net torque for all two-joint targets. Given the overall slower arm reaching speed, it is expected that the influence of interaction torque would be smaller compared to dynamic muscle torque. However, during movements towards targets T6 and T7 at the elbow, the dynamic muscle torque approached zero, suggesting that interaction torque played a more dominant role in these movements.

Notably, the key difference between the two groups emerges at the shoulder joint for targets T6 and T7, where the interaction torque contributed positively to the net torque. Compared to the control group, the cerebellar ataxia group exhibited a significantly lower contribution index of the interaction torque to the net torque at these targets. This suggests that the cerebellar group had difficulty utilizing interaction torque effectively to assist movement, leading to greater reliance on dynamic muscle torque, which may not fully compensate for the movement requirements of these complex, opposite joint movement tasks. (DMUS shoulder—T5: $F[1, 33] = 4.689$, $p = 0.038$, T6: $F[1, 33] = 19.346$, $p < 0.001$, T7: $F[1, 33] = 19.229$, $p < 0.001$; INT shoulder—T5: $F[1, 33] = 4.689$, $p = 0.038$, T6: $F[1, 33] = 19.346$, $p < 0.001$, T7: $F[1, 33] = 19.229$, $p < 0.001$; DMUS elbow— T5: $F[1, 33] = 8.585$, $p = 0.006$, T6: $F[1, 33] = 7.108$, $p < 0.012$; INT elbow— T5: $F[1, 33] = 8.585$, $p = 0.006$, T6: $F[1, 33] = 7.108$, $p < 0.012$).

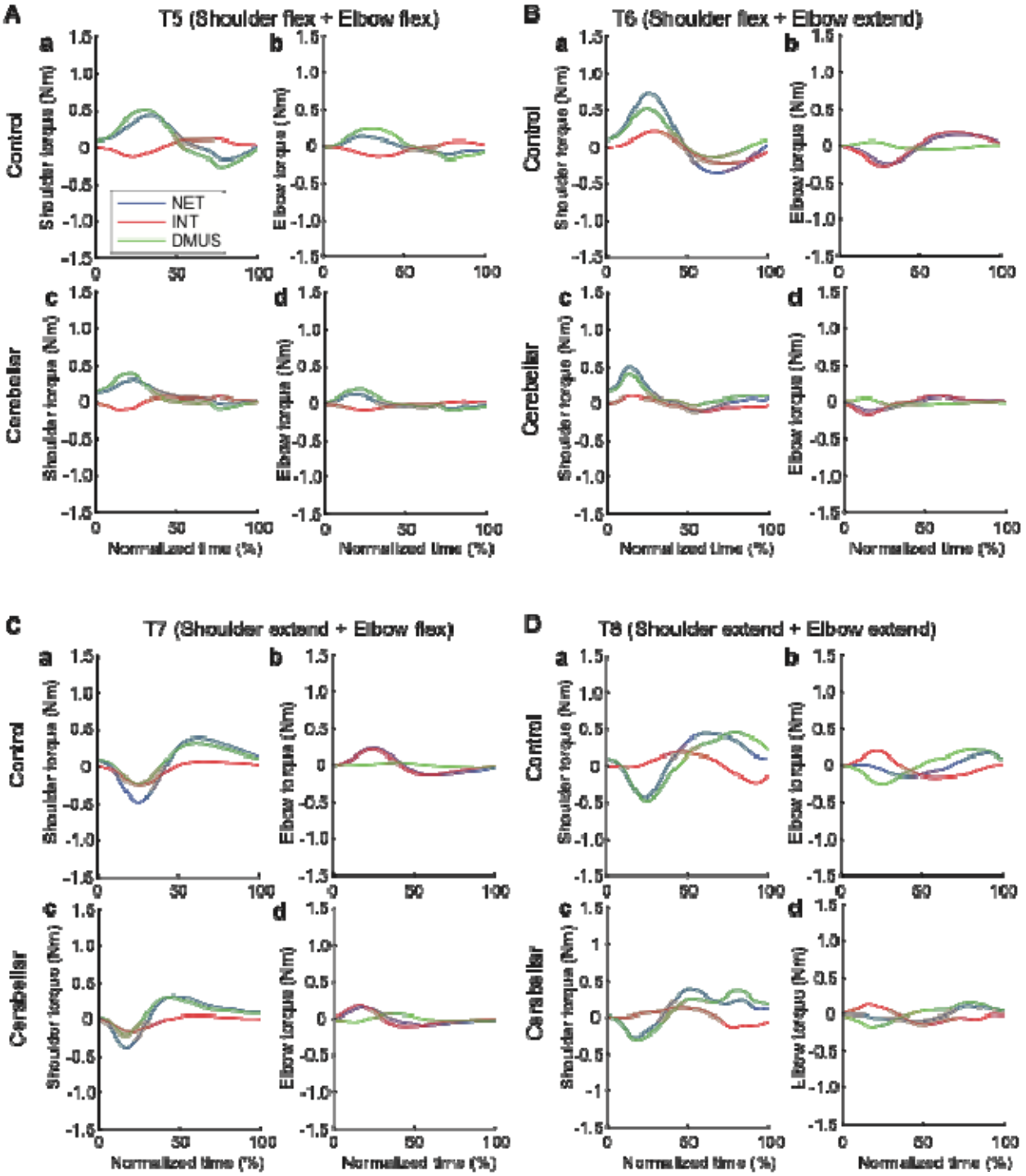

Figure 8. Group mean joint torque for two-joint targets: Target T5 (shoulder flexion and elbow flexion, A), target T6 (shoulder flexion and elbow extension, B), target T7 (shoulder extension and elbow flexion, C), and target T8 (shoulder extension and elbow extension, D). Panel a: shoulder joint torques in the control group. Panel b: elbow joint torques in the control group. Panel c: shoulder joint torques in the cerebellar ataxia group. Panel d: elbow joint torques in the cerebellar ataxia group.

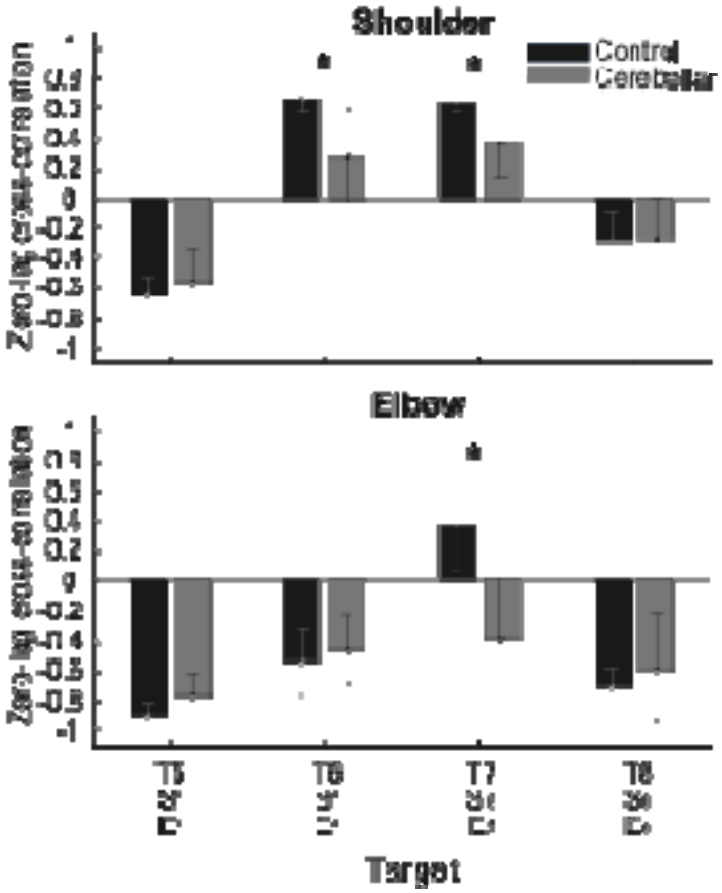

Figure 9. Zero-lag cross-correlation between dynamic muscle torque and interaction torque in the shoulder and elbow joints for two-joint targets (: $p < 0.05$)*

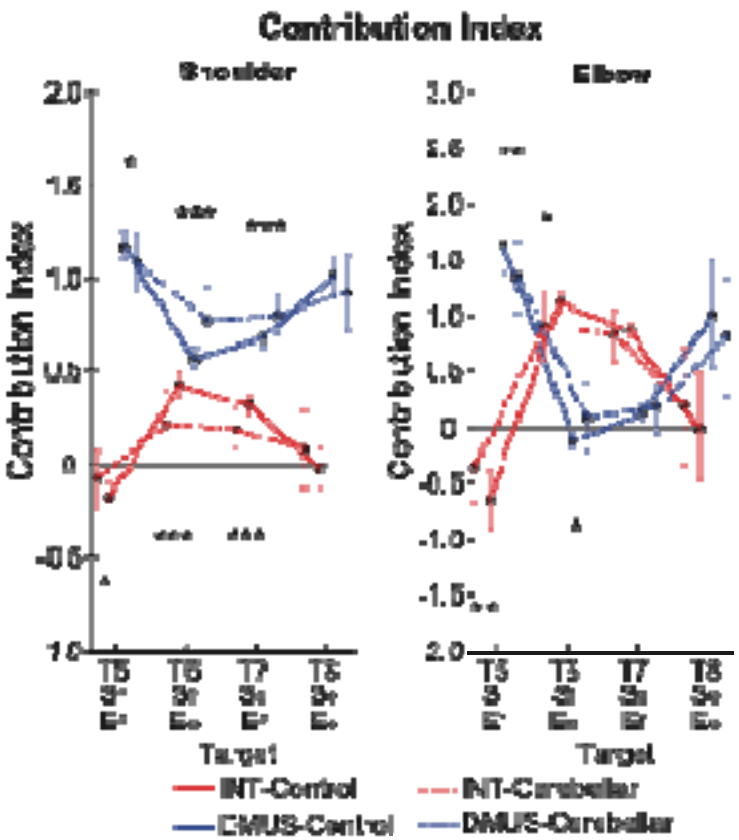

Figure 10. Contribution index. (: $p < 0.05$, **: $p < 0.01$, and ***: $p < 0.001$)*

Discussion

Here we asked if people with cerebellar damage have specific sensitivities to kinematic and dynamic demands during reaching. We studied people with cerebellar ataxia and matched controls reaching into targets in virtual reality using either single joint or two-joint arm movements. As expected, controls made near-straight hand trajectories to all targets, with low inter-subject variability. In contrast, cerebellar subjects made curved hand trajectories that varied across targets, with high inter-subject variability.

We were surprised to find that the cerebellar group had more impairment in the two-joint reaches that involved opponent joint movements compared to movements where both joints moved in the same direction. All two-joint reaches involve coordination between joints and generated interaction torques, so we expected them to be comparably impaired. Instead, we found that opponent two-joint reaches were more sensitive to kinematic timing demands compared to same-direction two-joint movements. Our kinematic simulation supports this—a similar error in joint onset times and rates of motion would manifest differently depending on whether the joint movements occur in the opposite or the same direction. For example, poor timing of opponent joint movements would not move the hand closer to the target and may even move the hand away from it. The same-direction joint movements tend to move the hand approximately towards the target so inter-joint timing matters less. Single joint reaches were

also less impaired for the cerebellar group, regardless of the joint used (elbow or shoulder) or direction of movement (flexion or extension).

We also found that the dynamics of the two-joint reaches were different. In opponent two-joint reaches, interaction torques assisted the movement—they were positively correlated with the dynamic muscle torques and worked together to generate the movement. The cerebellar group had difficulty taking advantage of the assistive interaction torques. Compared to controls, the cerebellar group showed lower correlations between interaction and dynamic muscle torques with smaller contributions of the interaction torques to overall joint movements. We speculate that assistive interaction torques would be difficult to incorporate into a movement if an individual has difficulty predicting how they will move the arm. The cerebellar group was better able to counter resistive interaction torques during same-direction two-joint reaches and during single jointed movements to stabilize the stationary joint. Resistive interaction torques may be easier for our cerebellar subjects to counter through feedback control in response to the perturbations that they cause (Zimmet et al. 2020).

Note that these deficits were not clearly related to the velocity of the reaching movements. It is well known that cerebellar subjects show greater deficits with faster movements (Bastian et al. 1996; Topka et al. 1998a). Here, the peak reach velocities varied depending on the reaching movement. This is because the hand-to-target distance varied with different combinations of 20° joint motions. However, the most impaired (i.e., opponent two-joint) reaches were shorter and thus hit lower peak velocities. Overall, we found that the peak hand velocities and acceleration times were not different between control and cerebellar groups, suggesting that speed was not the prime factor explaining our results. We did see longer hand deceleration times in the cerebellar group compared to controls, which has been previously reported particularly when end-point target accuracy is prioritized (Bastian et al. 1996; Brown et al. 1990) It is interesting that the reaches which were most difficult for our cerebellar group exhibited both features that we identified as problematic: greater kinematic temporal demands and assistive interaction torques. We think that both of these factors were important challenges for the cerebellar group, but our study does not allow us to determine which is most important. We hypothesize that either would make reaching harder to control. Future studies should design reaching tasks specifically to disentangle these factors more clearly. We also expect that the cerebellar participants may have more difficult controlling the interaction torques in faster movements where the dynamics demands become much more salient.

Home-based studies like these inevitably have some limitations. We reported that the cerebellar group showed out-of-plane movements that were small, but still larger than those that we saw in the control group. We acknowledge that this could introduce very small errors in our inverse kinematics calculations of sagittal plane joint motions, but did not affect our overall results. For example, a person who had the average arm length of our study participants (upper arm = 30 cm, lower arm and hand = 40 cm) at a posture with the elbow at 90° and the shoulder at 45° would have < 0.1° error at both joints if the hand moved 3 cm out of the sagittal plane. Another limitation is that the kinematic simulations were not perfectly matched with the human data. This is because our simulations used idealized joint movements that were based

on logistic fits of the average control group reaches. This simplification captures general patterns but does not account for the idiosyncrasies of how individual subjects move (e.g., changes in rate of joint motions during the reach). We feel that this method still provides a picture of the overall sensitivities of the different two-joint reaches. Finally, while the sampling rate of the oculus rift was lower than what we would typically use in the laboratory, it was more than sufficient to capture the self-paced reaches studied here.

In summary, the kinematic and dynamic results suggest that cerebellar subjects' reaching ataxia stems not only from impaired timing of joint motions but also from their inability to effectively harness assistive torques acting across joints. This inability to properly coordinate both kinematics and dynamics results in the observed pattern of reach trajectories. Thus, rehabilitation strategies that focus on enhancing both the timing of joint movements and the ability to manage interaction torques could be particularly beneficial for people with cerebellar ataxia.

Acknowledgements

This work was supported by National Institute of Health R01 HD040289 to A. J. Bastian.

REFERENCES

Alhussein L, Smith MA. 2021. Motor planning under uncertainty. Elife. 10.

Bastian AJ, Martin TA, Keating JG, Thach WT. 1996. Cerebellar ataxia: Abnormal control of interaction torques across multiple joints. J Neurophysiol. 76(1):492-509.

Bastian AJ, Thach WT. 1995. Cerebellar outflow lesions: A comparison of movement deficits resulting from lesions at the levels of the cerebellum and thalamus. Ann Neurol. 38(6):881-892.

Bastian AJ, Zackowski KM, Thach WT. 2000. Cerebellar ataxia: Torque deficiency or torque mismatch between joints? J Neurophysiol. 83(5):3019-3030.

Becker WJ, Morrice BL, Clark AW, Lee RG. 1991. Multi-joint reaching movements and eye-hand tracking in cerebellar incoordination: Investigation of a patient with complete loss of purkinje cells. Can J Neurol Sci. 18(4):476-487.

Bhanpuri NH, Okamura AM, Bastian AJ. 2014. Predicting and correcting ataxia using a model of cerebellar function. Brain. 137(Pt 7):1931-1944.

Brown SH, Hefter H, Mertens M, Freund HJ. 1990. Disturbances in human arm movement trajectory due to mild cerebellar dysfunction. J Neurol Neurosurg Psychiatry. 53(4):306-313.

Cashaback JG, McGregor HR, Gribble PL. 2015. The human motor system alters its reaching movement plan for task-irrelevant, positional forces. J Neurophysiol. 113(7):2137-2149.

Cusumano JP, Dingwell JB. 2013. Movement variability near goal equivalent manifolds: Fluctuations, control, and model-based analysis. Hum Mov Sci. 32(5):899-923.

Day BL, Thompson PD, Harding AE, Marsden CD. 1998. Influence of vision on upper limb reaching movements in patients with cerebellar ataxia. Brain. 121 (Pt 2):357-372.

Galloway JC, Koshland GF. 2002. General coordination of shoulder, elbow and wrist dynamics during multijoint arm movements. Exp Brain Res. 142(2):163-180.

Germanotta M, Vasco G, Petrarca M, Rossi S, Carniel S, Bertini E, Cappa P, Castelli E. 2015. Robotic and clinical evaluation of upper limb motor performance in patients with friedreich's ataxia: An observational study. J Neuroeng Rehabil. 12:41.

Gibo TL, Criscimagna-Hemminger SE, Okamura AM, Bastian AJ. 2013. Cerebellar motor learning: Are environment dynamics more important than error size? J Neurophysiol. 110(2):322-333.

Goodkin HP, Keating JG, Martin TA, Thach WT. 1993. Preserved simple and impaired compound movement after infarction in the territory of the superior cerebellar artery. Can J Neurol Sci. 20 Suppl 3:S93-104.

Gordon J, Ghilardi MF, Cooper SE, Ghez C. 1994. Accuracy of planar reaching movements. Ii. Systematic extent errors resulting from inertial anisotropy. Exp Brain Res. 99(1):112-130.

Gribble PL, Ostry DJ. 1999. Compensation for interaction torques during single- and multijoint limb movement. J Neurophysiol. 82(5):2310-2326.

Haggard P, Jenner J, Wing A. 1994. Coordination of aimed movements in a case of unilateral cerebellar damage. Neuropsychologia. 32(7):827-846.

Haith AM, Huberdeau DM, Krakauer JW. 2015. Hedging your bets: Intermediate movements as optimal behavior in the context of an incomplete decision. PLoS Comput Biol. 11(3):e1004171.

Hallett M, Massaquoi SG. 1993. Physiologic studies of dysmetria in patients with cerebellar deficits. Can J Neurol Sci. 20 Suppl 3:S83-92.

Hollerbach MJ, Flash T. 1982. Dynamic interactions between limb segments during planar arm movement. Biol Cybern. 44(1):67-77.

Maeda RS, Cluff T, Gribble PL, Pruszynski JA. 2017. Compensating for intersegmental dynamics across the shoulder, elbow, and wrist joints during feedforward and feedback control. J Neurophysiol. 118(4):1984-1997.

Maschke M, Gomez CM, Ebner TJ, Konczak J. 2004. Hereditary cerebellar ataxia progressively impairs force adaptation during goal-directed arm movements. J Neurophysiol. 91(1):230-238.

Reoli R, Therrien A, Millar J, Hill N, Varghese R, Roemmich R, Whitall J, Bastian A, Keller J. 2024. The scale for assessment and rating of ataxia is reliable and valid in the telehealth setting for patients with cerebellar ataxia. Phys Ther. 104(3).

Sainburg RL, Kalakanis D. 2000. Differences in control of limb dynamics during dominant and nondominant arm reaching. J Neurophysiol. 83(5):2661-2675.

Thach WT, Goodkin HP, Keating JG. 1992. The cerebellum and the adaptive coordination of movement. Annu Rev Neurosci. 15:403-442.

Therrien AS, Statton MA, Bastian AJ. 2021. Reinforcement signaling can be used to reduce elements of cerebellar reaching ataxia. Cerebellum. 20(1):62-73.

Topka H, Konczak J, Dichgans J. 1998a. Coordination of multi-joint arm movements in cerebellar ataxia: Analysis of hand and angular kinematics. Exp Brain Res. 119(4):483-492.

Topka H, Konczak J, Schneider K, Boose A, Dichgans J. 1998b. Multijoint arm movements in cerebellar ataxia: Abnormal control of movement dynamics. Exp Brain Res. 119(4):493-503.

Vu VH, Isableu B, Berret B. 2016. Adaptive use of interaction torque during arm reaching movement from the optimal control viewpoint. Sci Rep. 6:38845.

Winter D. 1990. *Biomechancis and motor control of human movement*. 2nd ed. New York: Wiley-Interscience.

Yamasaki H, Tagami Y, Fujisawa H, Hoshi F, Nagasaki H. 2008. Interaction torque contributes to planar reaching at slow speed. Biomed Eng Online. 7:27.

Zimmet AM, Cao D, Bastian AJ, Cowan NJ. 2020. Cerebellar patients have intact feedback control that can be leveraged to improve reaching. Elife. 9.

Zimmet AM, Cowan NJ, Bastian AJ. 2019. Patients with cerebellar ataxia do not benefit from limb weights. Cerebellum. 18(1):128-136.

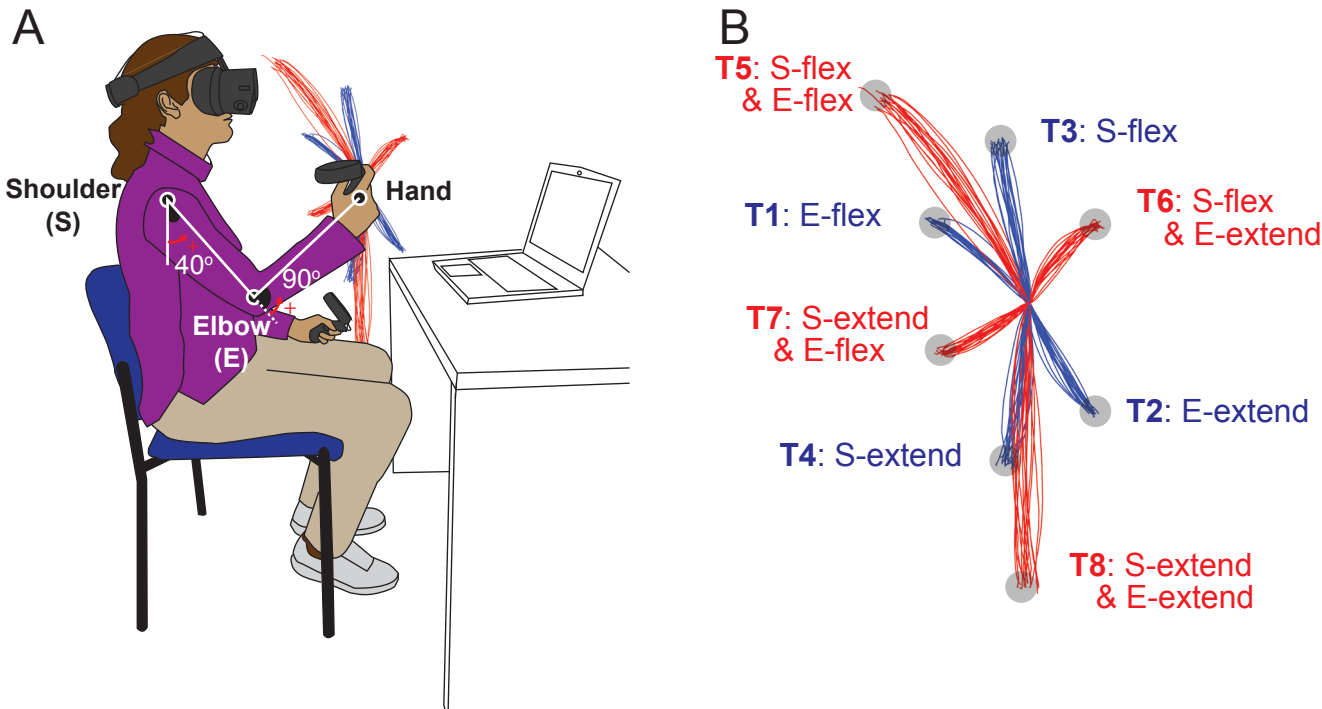
A
Shoulder
(S)
Hand
40°
90°
Elbow
(E)
B
T5: S-flex
& E-flex
T3: S-flex
T1: E-flex
T6: S-flex
& E-extend
T7: S-extend
& E-flex
T2: E-extend
T4: S-extend
T8: S-extend
& E-extend

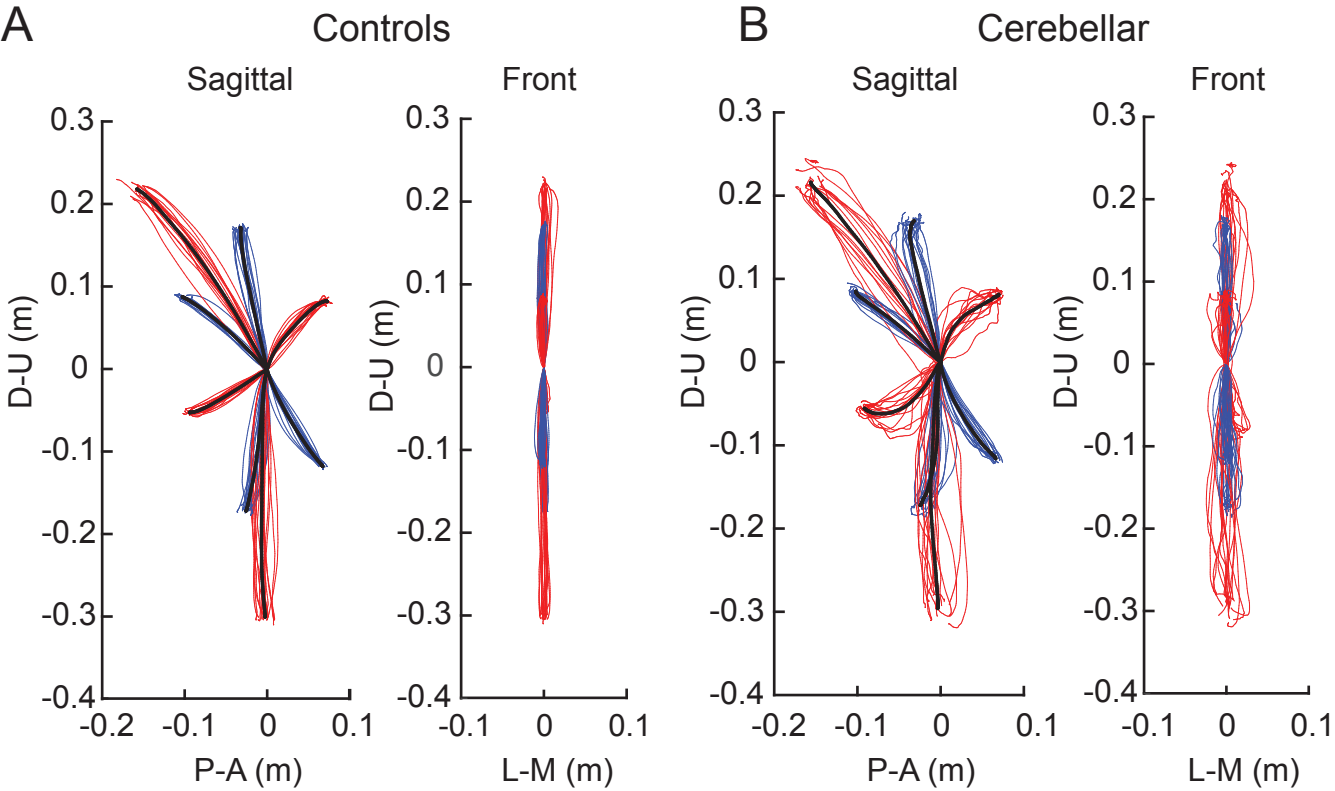
A
Controls
Sagittal
Front
B
Cerebellar
Sagittal
Front
D-U (m)
P-A (m)
L-M (m)
0.3
0.2
0.1
0
-0.1
-0.2
-0.3
-0.4
-0.2
-0.1
0
0.1

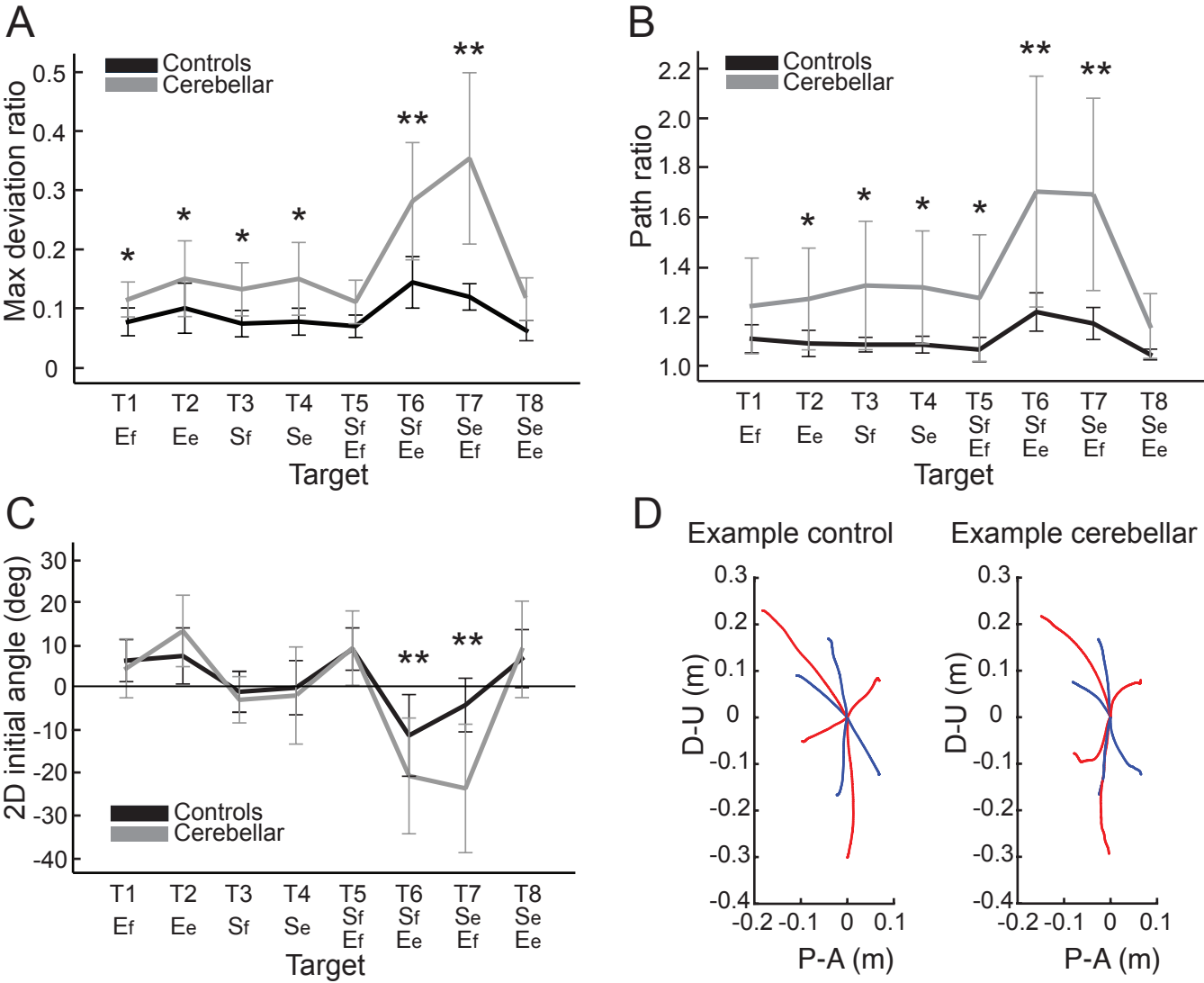
A
Controls
Cerebellar
Max deviation ratio
0.5
0.4
0.3
0.2
0.1
0
*
*
*
*
**
**
T1 Ef
T2 Ee
T3 Sf
T4 Se
T5 Sf Ef
T6 Sf Ee
T7 Se Ef
T8 Se Ee
Target
B
Controls
Cerebellar
Path ratio
2.2
2.0
1.8
1.6
1.4
1.2
1.0
*
*
*
*
**
**
T1 Ef
T2 Ee
T3 Sf
T4 Se
T5 Sf Ef
T6 Sf Ee
T7 Se Ef
T8 Se Ee
Target
C
2D initial angle (deg)
30
20
10
0
-10
-20
-30
-40
**
**
Controls
Cerebellar
T1 Ef
T2 Ee
T3 Sf
T4 Se
T5 Sf Ef
T6 Sf Ee
T7 Se Ef
T8 Se Ee
Target
D
Example control
Example cerebellar
D-U (m)
0.3
0.2
0.1
0
-0.1
-0.2
-0.3
-0.4
-0.2 -0.1 0 0.1
P-A (m)

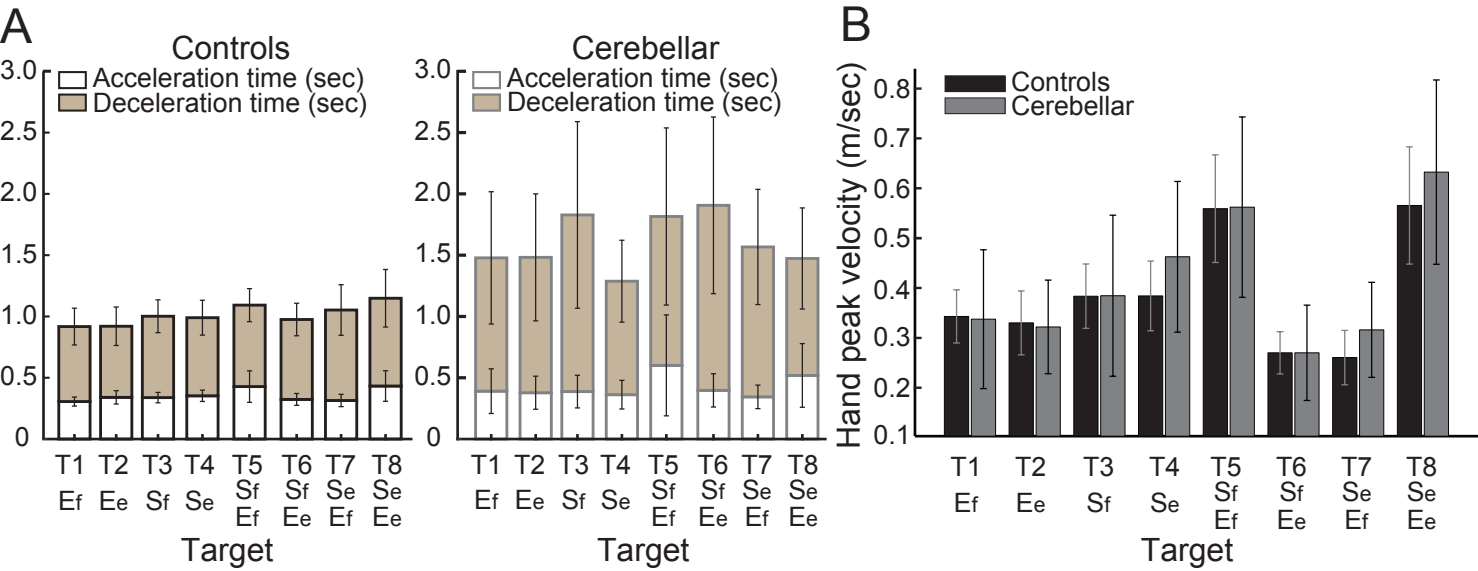
A
Controls
Acceleration time (sec)
Deceleration time (sec)
Cerebellar
Acceleration time (sec)
Deceleration time (sec)
3.0
2.5
2.0
1.5
1.0
0.5
0
T1 Ef
T2 Ee
T3 Sf
T4 Se
T5 Sf Ef
T6 Sf Ee
T7 Se Ef
T8 Se Ee
Target
B
Controls
Cerebellar
Hand peak velocity (m/sec)
0.8
0.7
0.6
0.5
0.4
0.3
0.2
0.1
T1 Ef
T2 Ee
T3 Sf
T4 Se
T5 Sf Ef
T6 Sf Ee
T7 Se Ef
T8 Se Ee
Target

A

Joint angle trajectories

Up = Flexion

Shouder (Control, Individual)
Elbow (Control, Individual)
Shoulder (Cerebellar, Individual)
Elbow (Cerebellar, Individual)
Shoulder (Control, Group)
Elbow (Control, Group)
Shoulder (Cerebellar, Group)
Elbow (Cerebellar, Group)

Controls | Cerebellar | Means only

T8 Se Ee
T7 Se Ef
T6 Sf Ee
T5 Sf Ef
T4 Se
T3 Sf
T2 Ee
T1 Ef

50 deg

0 50 100
Normalized time (%)

B

Joint angle variation at 50% of reaching time

Controls | Cerebellar

Shoulder
Elbow

Standard deviation (deg)
0 1 2 3 4

T1 Ef, T2 Ee, T3 Sf, T4 Se, T5 Sf Ef, T6 Sf Ee, T7 Se Ef, T8 Se Ee

Target

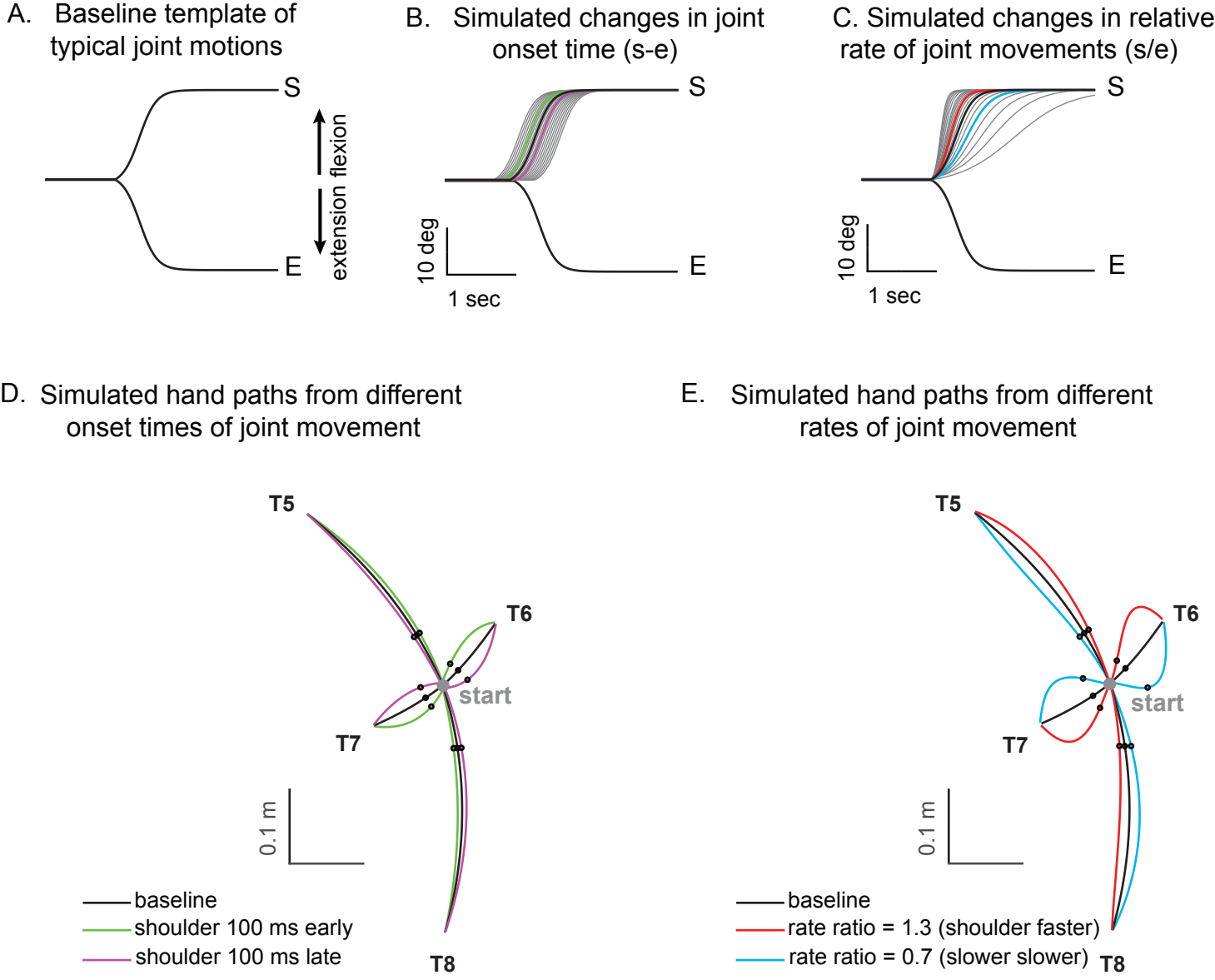
A. Baseline template of typical joint motions
S
E
extension flexion
B. Simulated changes in joint onset time (s-e)
S
E
10 deg
1 sec
C. Simulated changes in relative rate of joint movements (s/e)
S
E
10 deg
1 sec
D. Simulated hand paths from different onset times of joint movement
T5
T6
T7
T8
start
0.1 m
baseline
shoulder 100 ms early
shoulder 100 ms late
E. Simulated hand paths from different rates of joint movement
T5
T6
T7
T8
start
0.1 m
baseline
rate ratio = 1.3 (shoulder faster)
rate ratio = 0.7 (slower slower)

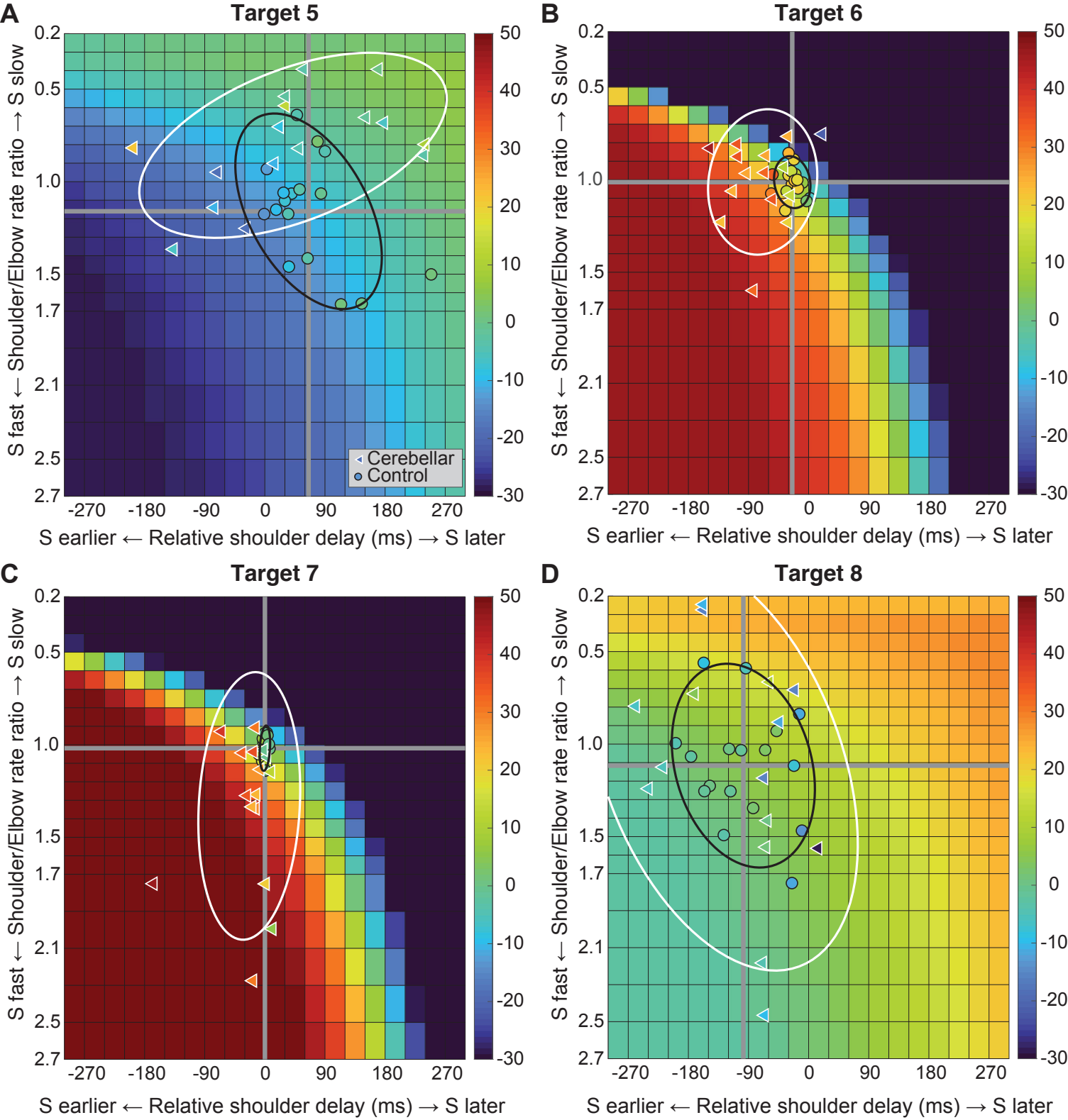
A
Target 5
B
Target 6
C
Target 7
D
Target 8
S fast ← Shoulder/Elbow rate ratio → S slow
0.2
0.5
1.0
1.5
1.7
2.1
2.5
2.7
-270
-180
-90
0
90
180
270
S earlier ← Relative shoulder delay (ms) → S later
50
40
30
20
10
0
-10
-20
-30
Cerebellar
Control

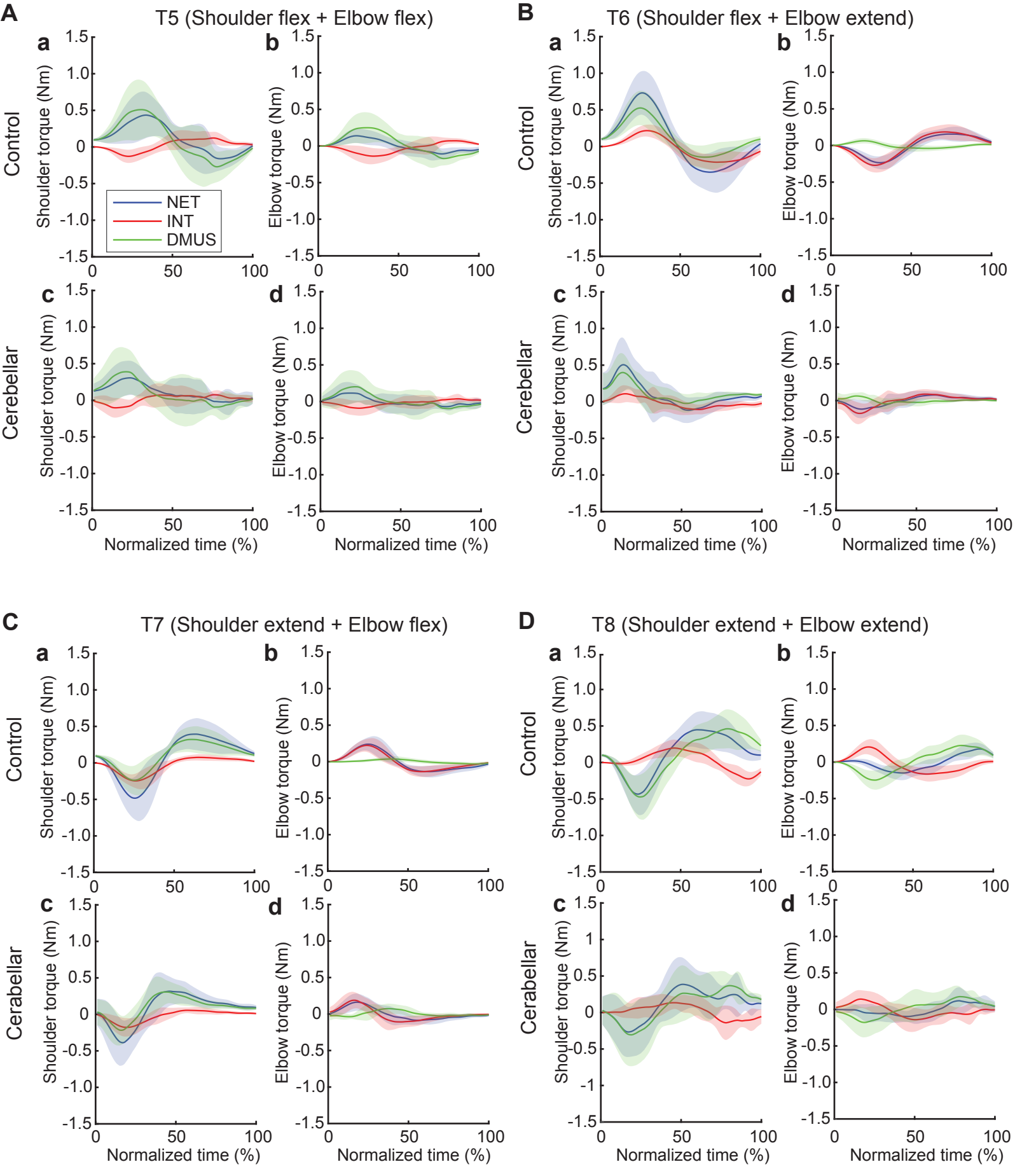
A
T5 (Shoulder flex + Elbow flex)
B
T6 (Shoulder flex + Elbow extend)
C
T7 (Shoulder extend + Elbow flex)
D
T8 (Shoulder extend + Elbow extend)
a
b
c
d
Control
Cerebellar
Cerabellar
Shoulder torque (Nm)
Elbow torque (Nm)
Normalized time (%)
NET
INT
DMUS

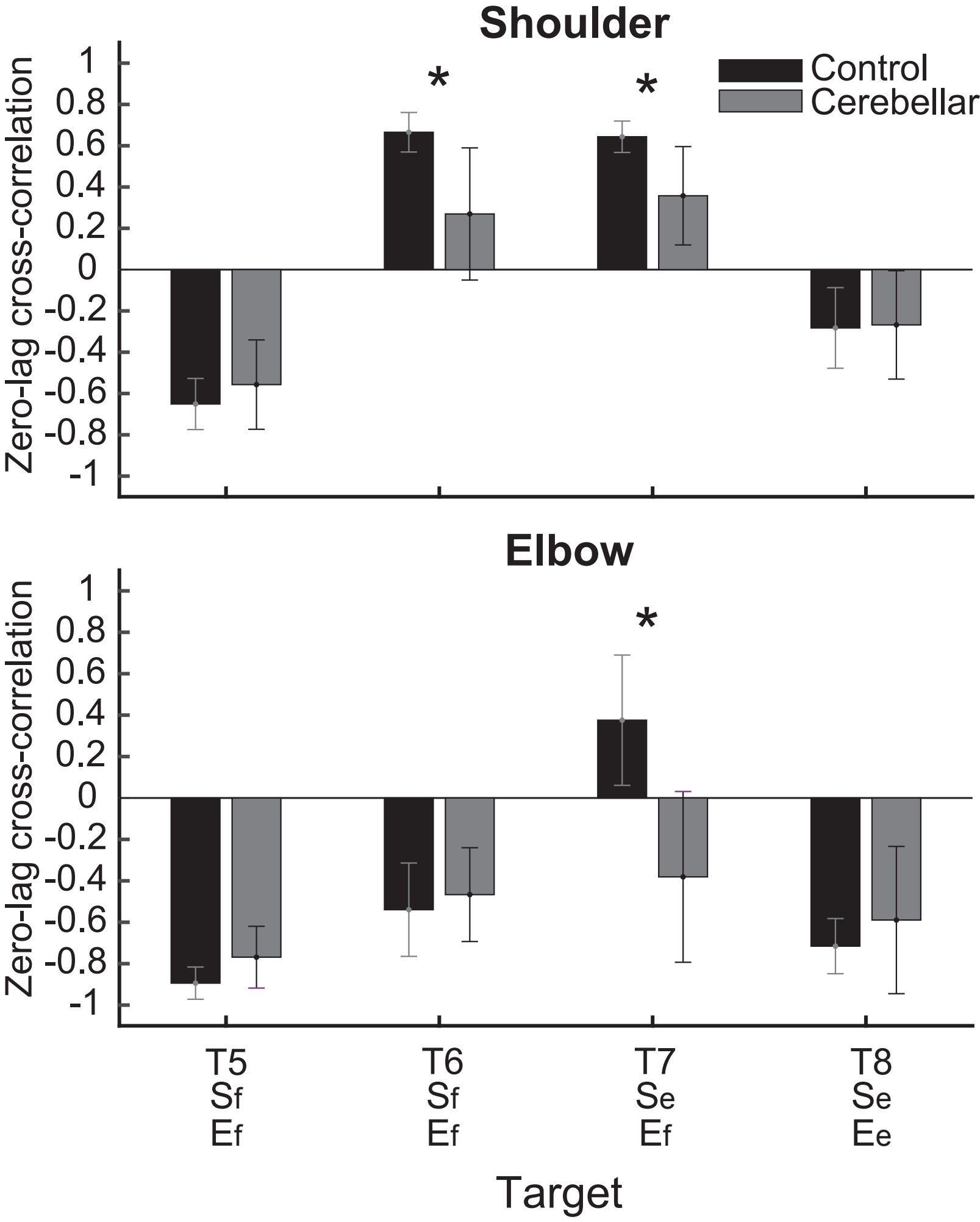
Shoulder
Control
Cerebellar
Zero-lag cross-correlation
1
0.8
0.6
0.4
0.2
0
-0.2
-0.4
-0.6
-0.8
-1
*
*
Elbow
Zero-lag cross-correlation
1
0.8
0.6
0.4
0.2
0
-0.2
-0.4
-0.6
-0.8
-1
*
T5
Sf
Ef
T6
Sf
Ef
T7
Se
Ef
T8
Se
Ee
Target

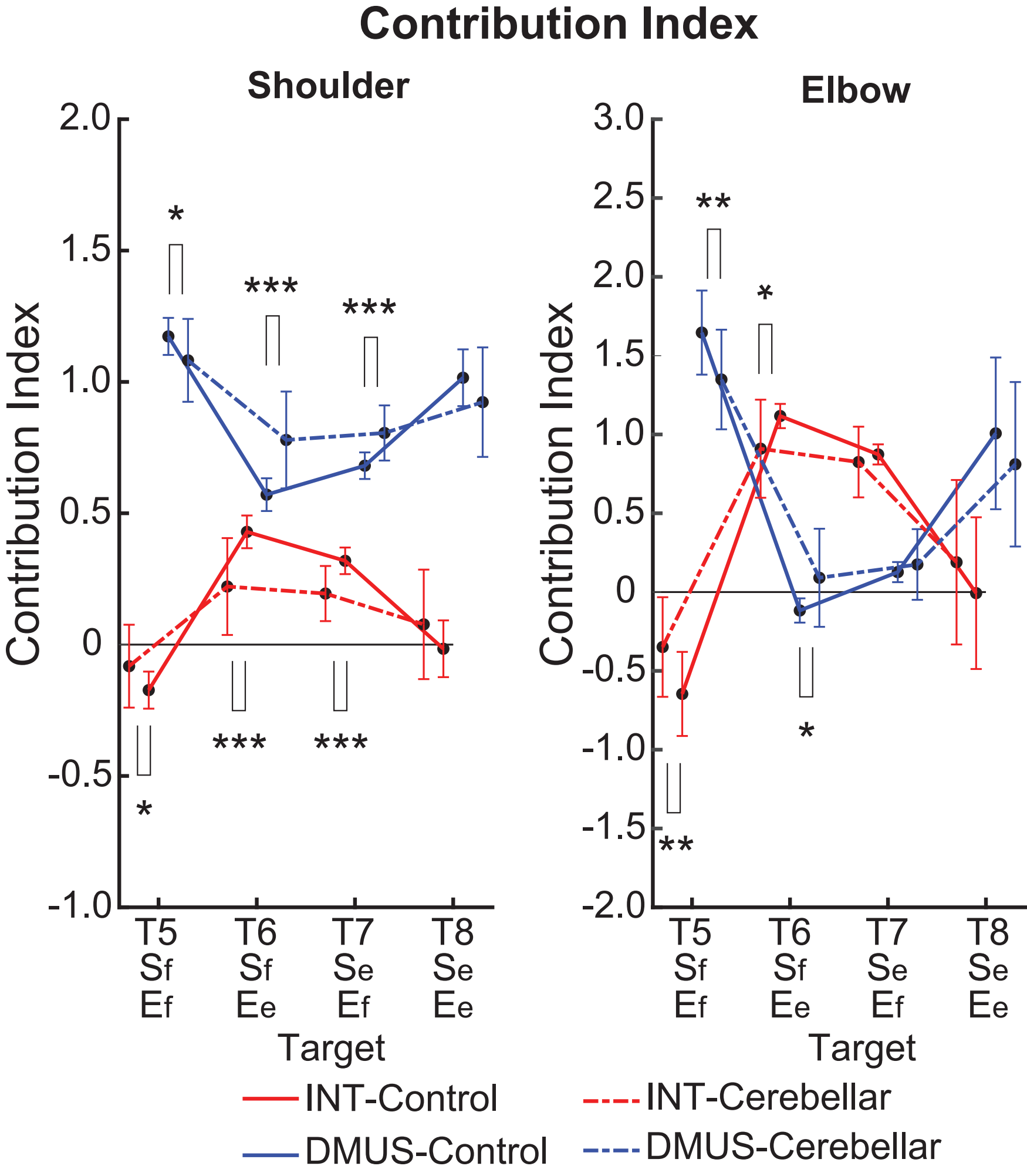
Contribution Index
Shoulder
Elbow
Contribution Index
2.0
1.5
1.0
0.5
0
-0.5
-1.0
3.0
2.5
2.0
1.5
1.0
0.5
0
-0.5
-1.0
-1.5
-2.0
*
***
***
*
***
***
**
*
*
**
T5 Sf Ef
T6 Sf Ee
T7 Se Ef
T8 Se Ee
Target
INT-Control
DMUS-Control
INT-Cerebellar
DMUS-Cerebellar